Stromal and Endothelial Transcriptional Changes during Progression from MGUS to Myeloma and after Treatment Response

Itziar Cenzano[1,2,*], Miguel Cócera[1,3,*], Marta Larrayoz[1], Lorea Campos-Dopazo[1], Sonia Sanz[1], Azari Bantan[2], Amaia Vilas-Zornoza[1,3], Patxi San-Martin[1], Paula Aguirre-Ruiz[1], Diego Alignani[1,3], Aitziber Lopez[1], Ignacio Sancho González[4,5], Javier Ruiz[5], Purificacion Ripalda-Cemborain[1], Marta Abengozar-Muela[6], Emma Muiños-López[1], Vincenzo Lagani[2,7,8], Jesper Tegner[2,9,10,11], Mikel Hernáez[3,12], Xabier Agirre[1,3], Benjamin Ebert[13], Bruno Paiva[1,3], Paula Rodriguez-Otero[3,14], Luis-Esteban Tamariz-Amador[3,14], Jesús San-Miguel[3,14], Borja Saez[1], José A. Martinez-Climent[1,3], Isabel A. Calvo[1,3,§], David Gomez-Cabrero[2,15,§], Felipe Prosper[1,3,14,§]

[1]Hematology and Oncology Program, Centre for Applied Medical Research (CIMA), Instituto de Investigaciones Sanitarias de Navarra (IdiSNA), Cancer Center Clinica Universidad de Navarra (CCUN), Pamplona, Spain.

[2]Bioscience Program, Biological and Environmental Sciences and Engineering Division (BESE), King Abdullah University of Science and Technology (KAUST), Thuwal, Saudi Arabia.

[3]Centro de Investigacion Biomedica en Red de Cancer (CIBERONC). Madrid, Spain.

[4]Hospital Reina Sofía de Tudela, Tudela, Spain.

[5]Hospital Universitario de Navarra, Instituto de Investigaciones Sanitarias de Navarra (IdiSNA), Pamplona, Spain.

[6]Departament of Pathology, Clinica Universidad de Navarra, Pamplona, Spain.

[7]SDAIA-KAUST Center of Excellence in Data Science and Artificial Intelligence, Thuwal, Saudi Arabia.

[8]Institute of Chemical Biology, Ilia State University, Tbilisi, Georgia.

[9]Computer Science Program, Electrical and Mathematical Sciences and Engineering Division, King Abdullah University of Science and Technology (KAUST), Thuwal, Saudi Arabia.

[10]Unit of Computational Medicine, Department of Medicine, Center for Molecular Medicine, Karolinska Institutet, Karolinska University Hospital, Stockholm, Sweden.

[11]Science for Life Laboratory, Solna, Sweden.

[12]Computational Biology Program. Cima Universidad de Navarra, Data Science and Artificial Intelligence Institute (DATAI) Universidad de Navarra, Instituto de Investigaciones Sanitarias de Navarra (IdiSNA). Pamplona, Spain.

[13]Department of Medical Oncology, Dana-Farber Cancer Institute, Harvard Medical School, Boston, United States of America.

[14]Hematology and Cell Therapy Department. Cancer Center Clinica Universidad de Navarra (CCUN), Instituto de Investigaciones Sanitarias de Navarra (IdiSNA). Pamplona, Spain.

[15]Translational Bioinformatics Unit, Navarrabiomed, Universidad Pública de Navarra (UPNA).

*These authors contributed equally to this work

[§]These authors jointly supervised this work

RUNNING TITLE: scRNA-seq of EC and MSC in MGUS and MM

KEYWORDS

Multiple myeloma, MGUS, single-cell RNA sequencing, Endothelial cells, Stromal cells, tumor microenvironment, mouse models and VRd treatment

CORRESPONDING AUTHOR

Felipe Prósper (fprosper@unav.es), David Gomez-Cabrero (david.gomezcabrero@kaust.edu.sa) and Isabel A. Calvo (icalvoa@unav.es).

For original data, please contact (icenzano@unav.es)

53 **ABSTRACT**

54 The role of the non-immune bone marrow microenvironment (BME) in the transition from monoclonal
55 gammopathy of undetermined significance (MGUS) into clinically active multiple myeloma (MM) remains
56 incompletely defined. To address this, we transcriptionally profiled endothelial cells (EC), mesenchymal stem
57 cells (MSC) and MM cells at single-cell resolution from two genetically engineered mouse models ($BI_{c\gamma1}$ and
58 $MI_{c\gamma1}$) that recapitulate MGUS to MM progression. Our analysis revealed distinct transcriptional trajectories
59 in EC and MSC, uncovering stage-specific BME–PC interactions shaping disease progression. EC acquired a
60 stress phenotype during MGUS transitioning to angiogenesis in MM, while MSC exhibited early impaired
61 differentiation capacity during MGUS that persisted in MM. Notably, an interferon (IFN)-associated MM
62 signature was detected in EC and MSC from the $BI_{c\gamma1}$ model but was absent in the more aggressive $MI_{c\gamma1}$
63 model. Treatment with bortezomib, lenalidomide, and dexamethasone remodeled the BME by suppressing
64 MM-IFN signaling, promoting an adaptive response in EC, and restoring osteogenic potential in MSC—
65 shifting the niche toward a less tumor-permissive state. Importantly, the MM-IFN signature was validated in
66 patients across the MGUS-to-MM spectrum, supporting the translational relevance of our findings. Together,
67 these data define novel dynamic and targetable alterations in the non-immune BME during myeloma
68 progression.

INTRODUCTION

Multiple myeloma (MM) is a B-cell malignancy characterized by the clonal expansion of plasma cells (PC) in the bone marrow (BM), preceded by asymptomatic precursor stages: monoclonal gammopathy of undetermined significance (MGUS) and smoldering multiple myeloma (SMM)[1]. Understanding the molecular mechanisms driving disease progression is crucial for developing therapies to prevent symptomatic MM.

The BM microenvironment (BME) comprises a complex network of hematopoietic and non-hematopoietic cells, extracellular matrix components, and soluble factors. This microenvironment creates an immunosuppressive and proinflammatory milieu that supports malignant PC growth and survival[2]. Therefore, the intricate interactions between myeloma cells and their surrounding microenvironment are crucial for developing effective therapies that can disrupt supportive signals and overcome drug resistance. While most studies have focused on the immune component[3–6], increasing evidence suggests that endothelial cells (EC) and mesenchymal stem cells (MSC) foster myeloma PC[7–9]. Furthermore, an enhanced inflammatory signature has been identified in MSC of MM patients[10–12]. However, the role of the non-hematopoietic BME to MGUS-to-MM progression remains poorly understood.

In this study, we took advantage of our recently described mouse models of MM that recapitulate the clinical, genetic, molecular, and immunological characteristics of MM patients[13]. These models include a precursor stage MGUS-like that progresses into symptomatic MM. Using single-cell RNA sequencing (scRNA-seq) data of Fluorescent-Activated Cell Sorted (FACS) non-hematopoietic BME cells and PC, we analyzed the transcriptional changes during disease transition and in response to current therapy. Our results identified distinct transcriptional dynamics between EC and MSC at the different stages of the disease. EC exhibited an altered vascular profile at MGUS, followed by the upregulation of angiogenesis pathways during MM. In contrast, MSC exhibited early downregulation of pathways associated with adhesion, osteogenic, and myogenic differentiation at the MGUS stage. Interestingly, we identified an interferon (IFN)-related myeloma signature in both EC and MSC that was reversed after treatment with bortezomib (Velcade®), lenalidomide (Revlimid®), and dexamethasone (VRd). Changes were validated in MSC from patients with MGUS, SMM, and MM, highlighting their potential role in disease progression.

97

98 **METHODS**

99 All detailed information is provided in supplemental methods.

100

101 ***Mice***

102 We used two genetically engineered MM mouse models, $BI_{c\gamma1}$ and $MI_{c\gamma1}$, that recapitulate the common features
103 observed in human MM. $YFP_{c\gamma1}$ mice were used as controls[13] (**Supplementary Table 1**). For each scRNA-
104 seq experiment at MGUS and MM-like stages, we used a pool of BM cells from 4-6 mice. In $BI_{c\gamma1}$ mice with
105 a humanized cereblon (CRBN)[14], VRd therapy was administered by oral gavage for 20 consecutive weeks.
106 The study included mice of both sexes and was approved by the Ethical Committee of Animal Experimentation
107 of the University of Navarra and the Health Department of the Navarra Government.

108

109 Murine BM non-hematopoietic cells were isolated as previously described[15] and sorted with GFP-positive
110 (GFP^+) PC using BD FACSAria II for subsequent scRNA-seq.

111

112 ***Human***

113 BM aspirates from individuals of both sexes with newly diagnosed MGUS (n = 5), SMM (n =2), or MM
114 (n =10), and bone-chip BM samples from healthy donors (HD) (50-80 years of age) HD (n=8) undergoing
115 orthopedic surgery were collected for bulk RNA-sequencing (bulk RNA-seq). Immunofluorescence (IF)
116 staining was performed on human BM biopsies from MGUS (n=4) and MM (n=7) patients, as well as on bone
117 chips from HD (n=2). Written informed consent was obtained according to the Declaration of Helsinki and the
118 Institutional Review Board of the University of Navarra. The clinical characteristics of all individuals are
119 described in **Supplementary Table 2**.

120

121 Samples were processed and BM cells were cryopreserved with FBS and 10% dimethyl sulfoxide (Sigma) in
122 liquid nitrogen until use. Frozen samples were thawed, and MSC were prospectively isolated and stored at -
123 80ºC for bulk RNA-seq.

124

125 ***Single-cell RNA and Bulk RNA sequencing***

126 Details on library preparation, sequencing, and additional information, including differential expression
127 analysis (DEA), gene ontology (GO) over-representation analysis (ORA), gene set enrichment analysis
128 (GSEA), cell-cell communication, and gene regulatory network (GRN) analysis, are described in supplemental
129 methods.

130

131 **RESULTS**

132 ***Single-cell transcriptomic profiling of BM murine cells in control, MGUS, and MM***

133 Using the $BI_{c\gamma1}$ myeloma model[13], we aimed to characterize transcriptional changes in BM stromal and EC
134 during transition from normal and precursor conditions to MM. This model, which carries BCL2 and $IKK2^{NF-}$
135 $^{\kappa B}$ genetic lesions triggered in germinal center B cells by a cre-cγ1 allele, develops signs of MGUS-like around
136 6 months of age that progressively evolves into MM within 4 to 6 months, overcoming limitations of previous
137 models. Considering that $BI_{c\gamma1}$ mice received T-cell-driven immunization, we included similarly immunized
138 $YFP_{c\gamma1}$ mice, carrying a yellow-fluorescence reporter activated from germinal-center B cells, as controls (**Fig.**
139 **1A**). We performed scRNA-seq on FACS-sorted non-hematopoietic BME cells (Lin^-, $TER119^-$, $CD45^-$, VDO^+,
140 and $7AAD^-$) and PC (VDO^+, $7AAD^-$ and GFP^+), yielding 12 437 cells (control=2 416, MGUS=4 169, MM=5
141 852) (**Supplementary Fig. 1**). Using canonical markers, we identified 17 clusters comprising EC, MSC, PC,
142 and other immune cells from the BME (**Fig. 1B**, **Supplementary Fig. 2A,B**). As a result, eight clusters were
143 labeled as PC (clusters PC1-8; n=7 924; markers: *Sdc1*, *Xbp1, Tnfrsf17,* and *Slamf7*); two clusters as
144 erythroblasts (Erythro1-2; n=457; *Hba-a1*, *Hba-a2, Car1,* and *Car2*); one cluster as neutrophils (n=176;
145 *S100a8*, *S100a9, Fcer1g,* and *Lyz2*); three clusters as EC (EC1-3; n= 3 288; *Cdh5*, *Cav1*, *Ly6c1*, and *Kdr*); and
146 two clusters as MSC (MSC1-2; n= 592; mesenchymal and osteolineage-primed markers *Cxcl12*, *Pdgfra*, *Lepr*,
147 and *Col1a2*) (**Fig. 1C, Supplementary Fig. 2C-F**).

148

149 To better understand the transcriptional shifts of MSC and EC during MM progression, these two cell
150 populations were analyzed separately (**Fig. 1D-G, Supplementary Fig. 2G-I)**. Overall, these results support
151 our cell enrichment strategy for isolating EC and MSC within the non-hematopoietic BME.

152

153 ***Identification of a MM-specific IFN signature in the BME***

154 Delving into the composition of EC, our analysis revealed a cluster of cells shared across all stages alongside
155 a second cluster ("MM2") that was nearly unique to the MM stage (**Fig. 2A**). Cells within the MM2 cluster
156 originated from both male and female mice, indicating that its emergence is not driven by a single animal
157 (**Supplementary Fig. 3**). The "MM2" cluster was characterized by the expression of IFN-inducible genes such
158 as *Ifit2*, *Rsad2*, *Ifit3*, *Isg15*, *Ifi44, Ifit,* and *Oasl2*, indicating an upregulation of an IFN response, as supported
159 by GO ORA (**Fig. 2B,C**).

160

161 To uncover the putative transcription factors (TFs) that might be underlying the IFN-like signature, we
162 performed GRN inference using SCENIC[16]. The study identified Irf7, Stat1, and Stat2 as potential master
163 regulators significantly activated in "MM2" EC (**Fig. 2D, Supplementary Fig. 4A-C**). These TFs are known
164 positive regulators of type I and type II IFN responses, which are associated with T cell immunosuppressive
165 function in MM patients[17].

166

167 To determine whether the IFN-like signature was unique for EC, we evaluated the signature score related to
168 "MM2" EC across other BM populations. This signature was also significantly upregulated in MM MSC at
169 the MM stage as well as PC, neutrophils, and erythroblasts, suggesting a shared immunomodulatory response
170 of the BME to the disease (**Fig. 2E,F, Supplementary Fig. 4D**). As the signature was not present in control
171 $YFP_{c\gamma1}$ mice or at precursor stages, we termed it MM-IFN signature to emphasize its association with the
172 myeloma stage. IF staining of BM samples from control $YFP_{c\gamma1}$ and $BI_{c\gamma1}$ mice at MGUS and MM stages,
173 validated the increased proportion of IFN^{+} EC and MSC in the MM stage (**Fig. 2G,H, Supplementary Fig.**
174 **4E)**.

175

176 Interestingly, when the MM-IFN signature was analyzed in the $MI_{c\gamma1}$ model[13], which carries MYC and $IKK2^{NF-}$
177 $^{\kappa B}$ from germinal-center B cells, no significant enrichment at any stage in either population was observed
178 (**Supplementary Fig. 4F-I).** This finding prompted us to investigate this MM-IFN signature in patients. The
179 analysis of the only publicly available dataset from MM patients[11] that contains non-immune BME uncovered
180 an enrichment of the murine MM-IFN signature in both EC and MSC from a subset of MM patients

181 (**Supplementary Fig. 4I-M**). Likewise, previous studies have described a similar IFN-inducible signature with
182 highly overlapping marker genes in PC and immune microenvironment cells from certain MM patients[3,4].
183 Collectively, our findings suggest that IFN-signaling is a coordinated response within the BME that could
184 define a subgroup of MM patients.
185
186 ***A stress pre-vascular state characterizes EC during the MGUS stage***
187 To investigate deeper the molecular mechanisms of myeloma progression, we analyzed the transcriptional
188 changes among EC at the different stages of the disease. An initial analysis uncovered a distinct transcriptome
189 profile of EC at the MGUS stage (**Fig. 3A**). MGUS EC overexpressed *Slpi*, *Hspa5*, *Mt1* and *Mt2*, indicating a
190 stress state at the onset of the disease related to protein folding, reticulum stress, and ion homeostasis (**Fig. 3B,**
191 **Supplementary Fig. 5A,B, Supplementary Table 3**). The upregulation of these genes may represent a "pre-
192 vascular phase" in the progression to MM. Moreover, *Cd74*, *Tmem176a,* and *Nme2*, were also overexpressed
193 in MGUS EC (**Supplementary Fig. 5C**). DEA between MGUS and non-IFN MM EC (n=1 193 cells)
194 identified 180 differentially expressed genes (DEGs) most of them upregulated (175 upregulated and 5
195 downregulated) (**Fig. 3C; Supplementary Table 4**), with MM EC showing a pro-vascular and lipid
196 metabolism profile (**Fig. 3D**). *Sox18*, a well described gene involved in tumor vascular development[18], as well
197 as *Fabp4* and *Cav1* were upregulated, suggesting their role in malignant transformation (**Supplementary Fig.**
198 **5D**). In the MGUS-like stage of the MIcγ1 model, we observed a stress-related transitional similar to that seen
199 in BIcγ1. However, MGUS MIcγ1 EC overexpressed genes of MM EC, indicating a stronger vascular
200 phenotype and faster progression (**Supplementary Fig. 6**).
201
202 Next, we identified and examined regulons of the $BI_{c\gamma1}$ model between MGUS and non-IFN MM EC. The
203 analysis revealed a decline in the activity of regulons during disease progression (**Fig. 3E, Supplementary**
204 **Fig. 7A,B**). Xbp1, which promotes endothelial proliferation via VEGF [19], showed the highest regulon activity
205 in MGUS EC, while Fos regulon was active at both stages. While Fos role has been previously described in
206 PC [20] our findings point to a potential regulatory role in EC as well (**Supplementary Fig. 7C,D**). Globally,
207 these findings suggest that MM-associated vascularization is preceded by a stress-related regulatory state in
208 MGUS EC, potentially contributing to disease progression.

209

210 ***MSC undergo early transcriptional changes during MGUS-like stage that persist in symptomatic MM***

211 Unlike EC, DEA indicated that MSC deregulation begins as early as the premalignant MGUS stage (**Fig. 4A**).
212 GSEA revealed impaired osteogenic and adipogenic differentiation capacity in MSC during MM development,
213 consistent with prior studies[8,10,21](**Fig. 4B, Supplementary Table 5**). Additionally, we identified
214 downregulation of muscle development genes, including *Pi16*, *Myl6*, *Enpp2, Nupr1*, and *Shox2*, which were
215 not previously linked to MM.

216

217 Given early changes at the MGUS stage, we compared MGUS and control MSC, identifying 409 DEGs (52
218 upregulated and 357 downregulated) (**Supplementary Table 6**). MGUS MSC exhibited enhanced expression
219 of genes and pathways related to oxidative phosphorylation, ATP metabolism, protein folding, and RNA
220 processing (**Fig. 4C,D**). Upregulation of *Cd74* in MGUS MSC and EC suggests its potential role in MM
221 progression. Only 35 DEGs were identified between MM and MGUS MSC (21 upregulated and 14
222 downregulated), further reflecting the high level of transcriptional similarity between both stages. Upregulated
223 genes in MM MSC were mainly related to immune response, consistent with the inflammatory profile in human
224 MM MSC[11] (**Fig. 4E,F, Supplementary Table 7).** Similar transcriptional changes were observed in MIcγ1
225 mice, supporting the impairment of MSC differentiation early in the MGUS-like stage (**Supplementary Fig.**
226 **8**).

227

228 Finally, a regulon analysis identified key TFs driving MSC alterations during MM progression (**Fig. 4G,**
229 **Supplementary Fig. 9A**). In control MSC Sp7, Dlx5, Sox8, Sox9, and Cebpa, well-known TFs mediating
230 osteochondrogenic and adipogenic differentiation, were identified. Reduced Klf4 activity supported impaired
231 myogenic potential in MGUS and MM MSC. Moreover, TFs from the AP-1 family and Egr1 showed the
232 highest regulon activity in MGUS MSC, consistent with their implication in MM development[22,23]. Yy1 and
233 Xbp1 regulons remained active from MGUS to MM, while Elk3 was specific to MM, suggesting its role in
234 cancer cell invasion[24–26] (**Supplementary Fig. 9B,C**). Overall, our results suggest that MSC undergo a TF-
235 mediated transcriptional shift at the MGUS stage that persists through disease progression.

236

237 ***Altered crosstalk between EC and MSC with malignant PC is potentially associated with myeloma***
238 ***development***
239 To further understand the mechanisms underlying BME-PC communication and how they may change upon
240 disease progression, we analyzed cellular communication through LIANA ligand-receptor (L-R) analysis[27]
241 (**Fig. 5A, Supplementary Fig. 10, Supplementary Table 8**). Interactions, through the *Fn1* ligand and *Insr*
242 receptor in EC and the *Cd93* PC receptor, were identified only in controls, while *Apoe* ligand in EC and *Adam9*,
243 *C3,* and *Vegfa* PC ligands were only found in MM (**Fig. 5B**). Our results support the role of angiogenesis in
244 myeloma via *Vegfa* secretion from PC, interacting with *Kdr*, *Nrp1*, and *Nrp2* in EC. High expression of Nrps
245 has been associated with tumor angiogenesis[28]. In addition, *Efna1-Epha8* interaction was predicted exclusively
246 in MM.
247
248 Interestingly, analysis of MSC-PC communication revealed interactions related to cell motility and adhesion
249 in MM that may be related to malignant PC extravasation (**Supplementary Fig. 10D)**. We observed a decrease
250 of *Thbs1-Itga4* and *Thbs2-Itga4* interactions, whereas MGUS and MM PC participate in outgoing interactions
251 involving *Mfge8* and *Sdc3*-mediated incoming interactions (**Fig. 5C**). Likewise, *Adam9,* which promotes
252 cancer egress and invasion[29], interacts with MSC through *Itgav* and *Itgb1* in MM.
253
254 We uncovered common L-R pairs between EC-PC and MSC-PC along disease progression (**Fig. 5D**). Multiple
255 interactions through the *Itgb5* PC receptor were initiated during MGUS. Moreover, in line with the previous
256 study in human MM patients[11], malignant PC interacted with MSC and EC through *Vegfa* secretion,
257 highlighting the role of angiogenesis in MM. Additionally, *C3*-mediated interactions between PC and the non-
258 hematopoietic BME in MM suggest that *C3* crosstalk maintains the immunosuppressive environment. Overall,
259 despite the limitations associated with the sparsity of single-cell resolution data and the limited number of cells
260 analyzed, the BME-PC interactions identified in the L-R based analysis are consistent with known pathways
261 associated with MM further identifying potential targets in the disease.
262
263 ***Treatment of MM mice with VRd induces a transcriptional remodeling of EC and MSC***

264 To assess the impact of MM therapy on EC and MSC molecular signatures, we performed scRNA-seq on a
265 pool of $BI_{c\gamma1}$ mice carrying humanized $CRBN^{I391V}$ ($BI_{c\gamma1}$-*Crbn*^{I391V})[14] after 20 weeks of treatment with VRd, a
266 current standard of care for patients with MM (**Supplementary Fig. 11A-D**). As expected, VRd treatment
267 significantly reduced the tumor burden and improved survival outcomes (**Supplementary Fig. 11E,F**). Given
268 the role of IFN signaling as a myeloma-specific response, we first sought to determine the presence of IFN
269 signature after treatment. Interestingly, VRd therapy downregulated IFN-driven MM signaling in EC and other
270 BM populations (**Fig. 6A, Supplementary Fig. 11G**). As a result, EC from treated mice exhibited decreased
271 expression of IFN-induced genes, such as *Ifit1, Ifit2, Gbp2*, and *Isg15*, and key related regulons previously
272 upregulated during myeloma development (**Supplementary Fig. 11H, Supplementary Table 9**). IF analysis
273 further confirmed the decrease in IFN^+ EC and MSC following VRd treatment, supporting a potential link
274 between IFN signaling suppression and the anti-myeloma drug response (**Fig. 6B,C, Supplementary Fig.
275 11I)**. To further explore the significance of our findings, we analyzed a publicly available bulk RNA-seq data
276 of MSC from MM patient samples before and after induction therapy with bortezomib-thalidomide-
277 dexamethasone with or without daratumumab[11]. This revealed a reduction of IFN- signature post-treatment in
278 high-IFN MM patients (**Supplementary Fig. 11J,K)**. Similarly, Chen et al.[6] reported a widespread
279 downregulation of IFN-response genes in immune cells following bortezomib-cyclophosphamide-
280 dexamethasone therapy, supporting the relevance of our results in the context of human disease.
281
282 Beyond dampening the IFN signature, VRd treatment induced broader gene expression changes in both EC
283 and MSC. In EC, DEA revealed upregulation of genes involved in mitochondrial metabolism, stress response,
284 detoxification, and chromatin remodeling—indicative of an adaptive response (**Fig. 6D,E)**. Consistent with its
285 known tumor-suppressive role and previous studies in MM cells after bortezomib exposure, *Klf2* was
286 upregulated in VRd-treated EC[30,31] (**Supplementary Fig. 11L)**. Furthermore, GRN analysis revealed enhanced
287 activity of Zbtb7a and Rarg regulons, reinforcing this adaptive response[32,33] (**Supplementary Fig. 12A)**.
288 Treated EC were enriched in thrombotic regulation pathways, including upregulation of *Hmgb1*, a gene linked
289 to MM drug resistance[34] (**Supplementary Fig. 12B**). Consistent with lenalidomide's anti-angiogenic
290 effects[35,36], vascular and adhesion-related genes, including *Nrp1*, were downregulated and Xbp1 regulon
291 activity was reduced (**Supplementary Fig. 12A)**.

292

293 In MSC, VRd treatment downregulated immune and IFN signaling pathways, indicating reduced inflammation
294 in the BME (**Fig. 6F)**. Likewise, antigen presentation genes, such as *Cd74*, *B2m* and *Psmb8* were
295 downregulated (**Fig. 6G, Supplementary Table 10)**. Interestingly, decreased expression of *Mdm4* and *Cyba*
296 in treated MSC suggests that VRd may impair the proliferative supportive capacity of MSC[37,38]
297 (**Supplementary Fig. 12C)**. On the contrary, genes linked to ECM organization, wound healing, and bone
298 development were upregulated, aligning with bortezomib's anabolic effects[39,40] **(Supplementary Fig. 12D).**
299 GRN analysis confirmed osteogenic reprogramming via reactivation of Cebpa, Nfib, Nfic, Churc1 and Sox4
300 regulons (**Supplementary Fig. 12E)**. Finally, MSC-PC communication analysis identified interactions
301 previously observed in control MSC such as *Adam10–Tspan5*, *Adam17–Il6ra* and *Wnt10a–Fzd1/Lrp6* which
302 may contribute to anti-inflammatory and osteogenic adaptations following VRd treatment[41–44]
303 (**Supplementary Fig. 12F)**. Overall, our results suggest that VRd therapy suppresses IFN-driven MM
304 signaling and reprograms the BM niche by triggering an adaptive response in EC and restoring MSC
305 osteogenic potential, creating a less tumor-permissive BME.

306

307 ***Transcriptional dynamics of human MSC during myeloma progression***

308 To validate our findings in mice, we performed bulk RNA-seq in FACS-isolated MSC from aged-matched HD
309 (n = 8), newly diagnosed MGUS (n = 5), SMM (n =2), or MM (n =10) patients (**Fig. 7A, Supplementary Fig.**
310 **13A**). PCA revealed a distinction between MM-MSC and HD-MSC, with MGUS-MSC and SMM-MSC
311 mapped between them, showing an evolving transcriptional trajectory (**Fig. 7B**).

312

313 The comparison between MGUS-MSC and HD-MSC revealed 180 DEGs (120 upregulated and 60
314 downregulated) (**Fig. 7C, Supplementary Fig. 13B, Supplementary Table 11**). Downregulation of genes
315 related to osteoblast differentiation, such as *TNN, SPP1,* and *A2M,* indicate the early remodeling of MSC
316 previously described in our mouse data. Besides, MGUS-MSC upregulated genes related to cell cycle, protein
317 ubiquitination, ATP metabolism, and oxidative stress supporting their role in MM pathogenesis
318 (**Supplementary Fig. 13C**).

319

320 Consistent with the high transcriptional similarity observed in mice between MGUS and MM MSC, the fewest
321 DEGs were yielded when comparing MGUS and MM-MSC (41 upregulated and 33 downregulated) (**Fig. 7C**
322 **, Supplementary Fig. 13D, Supplementary Table 12**). MM-MSC showed enrichment in inflammatory-
323 related processes, indicating that a pro-inflammatory microenvironment is required for the transition between
324 premalignant stages and MM, in line with previous studies[12,45]. In addition, MM-MSC over-expressed
325 *PHLDA1*, *FOXC2*, *PPA1*, and *CTNNB1,* genes associated with Epithelial-Mesenchymal Transition (EMT),
326 which aligns with MSC potential to induce EMT through extracellular vesicles in MM[46] (**Supplementary Fig.**
327 **13D,E)**.
328
329 Defective osteogenic differentiation and dysfunctional immunomodulatory ability were confirmed when
330 comparing MM- vs HD-MSC (448 upregulated and 566 downregulated) (**Fig. 7C, Supplementary Fig.**
331 **13F,G, Supplementary Table 13)**. Furthermore, consistent with the impaired myogenic phenotype observed
332 in mice, human MM-MSC showed downregulation of muscle-related genes. GSEA revealed enrichment of
333 TNF-α signaling via NF-KB and IFN response in MM-MSC (**Fig. 7D)**. Interestingly, the IFN signature
334 previously identified in murine MM BME was enriched in a subset of MM patients, as shown in the analysis
335 of publicly available data from de Jong et al.[45] (**Fig. 7E, Supplementary Fig. 4I-L, Supplementary Fig.**
336 **11J,K, Supplementary Fig. 13H**). IF staining of BM samples from MGUS and MM patients showed an
337 enrichment of IFN-driven MM signaling in MSC from a subset of MM patients, further supporting our
338 transcriptional findings (**Fig. 7F,G, Supplementary Fig. 14A,B)**.
339
340 Finally, we determined changes in TF activity during myeloma progression (**Fig. 7H**). Enhanced activity of
341 TFs related to the NF-KB pathway, such as NF-KB, NKFB1, and RELA, were observed in MSC from both
342 MGUS and MM patients, highlighting NF-κB activation as an early event in MM evolution. Furthermore,
343 MM-MSC exhibited increased activity of IRF1 and IRF3, which again emphasizes the importance of IFN
344 signaling for the disease. In conclusion, the transcriptional changes of MSC between MSC from healthy
345 donors, MGUS and MM patients mirrors our findings in mouse models.
346
347 **DISCUSSION**

348 Over the last decades, our understanding of MM biology has advanced significantly[47–51], explicitly revealing
349 the contribution of the BME to the outgrowth and relapse of this hematological cancer and exerting a
350 supportive function for the expansion of malignant PC[3,11,52–54]. However, research has mainly concentrated on
351 PC and their immune microenvironment, highlighting the need for additional exploration of the non-
352 hematopoietic BME[9,55–57]. Here, using our validated $BI_{c\gamma1}$ and $MI_{c\gamma1}$ murine models[13], that closely mimic key
353 features of human MM progression, we provided a comprehensive overview of transcriptional deregulation in
354 EC and MSC during the transition from healthy to MGUS and MM as well as the reshaping of the non-
355 hematopoietic BME in response to VRd treatment. Further, we validated our results in MSC from MM patients
356 at various disease stages, both in our own data as well as in the only publicly available single cell MM patient
357 dataset[11].
358
359 Through analysis of the transcriptomic alterations along disease progression, we uncovered a pre-vascular state
360 in MGUS EC linked to protein folding and ion homeostasis, where upregulation of *Slpi*, *Mt1*, *Mt2*, and *Hspa5*,
361 could potentially serve as an early myeloma fingerprint in EC. Disease progression from MGUS to MM in EC
362 involved angiogenesis, migration, and metabolic shifts. Xbp1 and Fos, key regulators of vascular development
363 and cancer progression[19,20], showed enhanced activity with myeloma progression highlighting their potential
364 as disease targets. In contrast, transcriptional changes in MSC previously described in advanced MM
365 patients[8,10], were already present during the precursor MGUS-like stage. In addition to impaired osteogenic
366 differentiation, MGUS MSC exhibited a downregulation of myogenesis-related genes. Consistent with these
367 murine findings, our bulk RNA-seq showed impaired MSC differentiation in human patients, even at
368 premalignant stages. Similarly, MGUS prompted a metabolic swift in human MSC with increased protein
369 folding. These findings suggest that MGUS MSC show a reshaping of their differentiation capacity and
370 metabolism to support the growth of MM cells from the early stages of the disease.
371
372 Understanding the crosstalk between the BME and PC is crucial for unraveling tumor progression mechanisms,
373 and this study contributes to understand the interactions between EC, MSC, and malignant PC along the disease
374 evolution. Consistent with a previous study in MM patients[11], we found *Vegfa* secretion from PC as a hallmark
375 of MM angiogenesis through the interaction with *Kdr*, *Nrp1*, and *Nrp2* endothelial receptors. Additionally,

376 identifying *Efna1-Epha8* interaction exclusively in MM implicates the ephrin pathway in disease development,
377 as previously described in other cancers[58]. MSC-PC interactions were linked to adhesion, matrix organization,
378 and migration, suggesting MSC-PC crosstalk is crucial for MM extravasation and disease dissemination.
379
380 A fundamental finding of our study is the identification of a myeloma-specific IFN signature in EC that extends
381 to MSC and other BM cells, indicating a shared BME response during MM progression. This signature, that
382 differs from the inflammatory phenotype via TNFα and NF-κB described by de Jong et al.[11], is marked by
383 upregulation of IFN-inducible genes and master regulators (Irf7, Stat1, Stat2). STAT1/2 signaling, closely
384 linked to IFN in MM, supports tumor-promoting roles, complementing *STAT3*'s known oncogenic function in
385 MM migration and BM homing[59]. While prior scRNA-seq studies reported IFN activity in PC and immune
386 cells[3,4], only limited evidence suggested an IFNα response in MSC[9,55]. The MM IFN-inducible response
387 uncovered in our study, reveals an immunomodulatory role of the non-hematopoietic BME, with EC and MSC
388 potentially contributing to immune remodeling and T-cell exhaustion under inflammatory conditions[17].
389
390 Our findings expand on the concept of pro-inflammatory signaling within MM MSC[11], identifying an
391 enrichment of this IFN signature in both EC and MSC from a subset of MM patients, highlighting its clinical
392 relevance for patient stratification based on inflammatory features. More importantly, the suppression of this
393 MM-IFN signature in human MM patients after induction therapy, further supports its clinical relevance. In
394 addition, using our MGUS-MM mouse models, we demonstrate that VRd treatment impacts the non-
395 hematopoietic BME by suppressing this MM IFN signaling. While combinatorial regimens improve outcomes
396 in patients by targeting multiple pathways our results support their potential to reshape the BME[60] by inducing
397 and adaptive stress in EC, and restoring MSC osteogenic potential, shifting the niche toward a less tumor-
398 permissive state. These findings highlight the importance of targeting BME interactions and enhancing anti-
399 myeloma immune responses.
400
401 In summary, the use of the $BI_{c\gamma1}$ myeloma murine model, which mimics MGUS-to-MM progression, alongside
402 scRNA-seq, has enabled a comprehensive dissection of the non-hematopoietic BME. The myeloma-specific
403 IFN signature, the transition stress state in MGUS EC, the early transcriptional shifts in MSC, the evolving

404 cellular communication networks and the IFN signaling repression post-VRd therapy collectively support the
405 role of EC and MSC in MM development and treatment response. Validation in human patients reinforces the
406 study's translational relevance, suggesting that non-hematopoietic BME changes may foster MM development
407 from premalignant stages and shift toward a less tumor-permissive state after treatment.

408 **ACKNOWLEDGEMENTS**

409 This work was supported by the Instituto de Salud Carlos III and co-financed by ERDF A way of
410 making Europe (PI20/01308, PI22/00983, PI23/00516); CIBERONC (CB16/12/00489), RICORS
411 TERAV (RD21/0017/0009); Departamento de Industria Gobierno de Navarra (AGATA 0011-1411-
412 2020-000010/0011-1411-2020-000011) and Departamento de Salud Gobierno de Navarra; the
413 Cancer Research UK [C355/A26819]; FC AECC and AIRC under the Accelerator Award Program;
414 The International Myeloma Foundation (Brian van Novis) and The Paula and Rodger Riney
415 Foundation to FP. The study was also supported by The Spanish Government, through project
416 PID2019-111192GA-I00 (MICINN) to DGC. IAC was supported by Marie Curie grant (H2020-
417 MSCA-IF-837491) from European Commission. IC was supported by AECC predoctoral fellowship
418 (PRDNA19006CENZ). MC was supported by FPU fellowship (FPU22/03283) from Ministerio de
419 Ciencia, Innovación y Universidades.

420

421 We would like to thank the staff of the flow cytometry core, the advanced genomic lab, and the animal
422 facility at CIMA Universidad de Navarra for their invaluable technical and intellectual assistance.
423 We also acknowledge Hospital Reina Sofía de Tudela, Hospital Universitario de Navarra, the
424 Biobank of the University of Navarra, and Goretti Ariz for the provision of BM samples and their
425 collaboration. We are particularly grateful to the patients and healthy donors for their participation in
426 this study.

427

428 **AUTHORSHIP CONTRIBUTIONS**

429 I.C., M.C., L.C-D. and I.A.C. processed murine and human BM samples; B.S. and I.A.C.
430 conceptualized the study and analyzed the scRNA-seq experiments data; I.C., M.C., and I.A.C.
431 interpreted the scRNA-seq experiments data; I.C. and I.A.C. wrote the paper; M.C. analyzed the bulk
432 RNA-seq experiments data; M.C. and I.A.C. interpreted the bulk RNA-seq experiments data; M.L.

433 and J.A.M.C. designed and provided the mice models; M.L. and S.S. performed the VRd treatment
434 experiments. A.B. performed the cell-cell computational analysis; A.V., P.S.M., and P.A.R.
435 performed the scRNA-seq and bulk RNA-seq experiments. D.A. and A.L. performed the FACS
436 sorting. I.S.G. and J.R. provided the BM samples from HD; M.C., L.C-D. and P.R-C. conducted the
437 histologic experiments; M.C. analyzed the histologic experiments; M.A-M. and E.M. provided the
438 human MGUS and MM samples. D.G.C., with help from M.H. and J.T., supervised the computational
439 work. B.E. provided the humanized mouse model; B.P. and J.S-M. helped with the clinical data;
440 P.R.O. and L.E.T-A. provided the BM samples from MGUS, SMM, and MM patients; I.A.C. and
441 B.S. designed the research experiments; F.P., D.G.C. and I.A.C. conceived and directed the research
442 project.
443
444 All authors actively participated in the discussions underlying this manuscript. I.C., M.C., I.A.C.,
445 D.G.C., and F.P. discussed the results and wrote the final manuscript. All authors contributed to, read,
446 and approved the final manuscript.
447
448 **DISCLOSURE OF CONFLICTS OF INTEREST**
449 A patent on the knowhow and experimental use of the $BI_{c\gamma1}$ and $MI_{c\gamma1}$ mouse models of MM has been
450 licensed to MIMO Biosciences. J.A.M.-C. has received research funding from Roche-Genentech,
451 Bristol Myers Squibb, Janssen, Regeneron, Priothera Pharmaceuticals, Palleon Pharmaceuticals,
452 AstraZeneca, and K36 Therapeutics, and is founder and holds stock options of MIMO Biosciences.
453 The authors declare no competing interests.

454 **REFERENCES**

455 1 Kumar SK, Rajkumar V, Kyle RA, van Duin M, Sonneveld P, Mateos M-V *et al.* Multiple
456 myeloma. *Nat Rev Dis Primers* 2017; **3**: 17046.
457 2 Lomas OC, Tahri S, Ghobrial IM. The microenvironment in myeloma. *Curr Opin Oncol*
458 2020; **32**: 170–175.
459 3 Zavidij O, Haradhvala NJ, Mouhieddine TH, Sklavenitis-Pistofidis R, Cai S, Reidy M *et al.*
460 Single-cell RNA sequencing reveals compromised immune microenvironment in precursor
461 stages of multiple myeloma. *Nature Cancer 2020 1:5* 2020; **1**: 493–506.
462 4 Boiarsky R, Haradhvala NJ, Alberge JB, Sklavenitis-Pistofidis R, Mouhieddine TH, Zavidij
463 O *et al.* Single cell characterization of myeloma and its precursor conditions reveals
464 transcriptional signatures of early tumorigenesis. *Nature Communications 2022 13:1* 2022;
465 **13**: 1–15.
466 5 Pilcher W, Thomas BE, Bhasin SS, Jayasinghe RG, Yao L, Gonzalez-Kozlova E *et al.* Cross
467 center single-cell RNA sequencing study of the immune microenvironment in rapid
468 progressing multiple myeloma. *npj Genomic Medicine 2023 8:1* 2023; **8**: 1–18.
469 6 Chen M, Wan Y, Li X, Xiang J, Chen X, Jiang J *et al.* Dynamic single-cell RNA-seq analysis
470 reveals distinct tumor program associated with microenvironmental remodeling and drug
471 sensitivity in multiple myeloma. *Cell Biosci* 2023; **13**: 1–18.
472 7 García-Ortiz A, Rodríguez-García Y, Encinas J, Maroto-Martín E, Castellano E, Teixidó J *et*
473 *al.* The Role of Tumor Microenvironment in Multiple Myeloma Development and
474 Progression. *Cancers (Basel)* 2021; **13**: 217.
475 8 Maiso P, Mogollón P, Ocio EM, Garayoa M. Bone Marrow Mesenchymal Stromal Cells in
476 Multiple Myeloma: Their Role as Active Contributors to Myeloma Progression. *Cancers*
477 *2021, Vol 13, Page 2542* 2021; **13**: 2542.
478 9 Ghamlouch H, Gagler DC, Blaney P, Boyle EM, Wang Y, Avigan J *et al.* A proinflammatory
479 response and polarized differentiation of stromal elements characterizes the murine myeloma
480 bone marrow niche. *Exp Hematol Oncol* 2025; **14**. doi:10.1186/S40164-025-00606-X.
481 10 Alameda D, Saez B, Lara-Astiaso D, Sarvide S, Lasa M, Alignani D *et al.* Characterization
482 of freshly isolated bone marrow mesenchymal stromal cells from healthy donors and patients
483 with multiple myeloma: transcriptional modulation of the microenvironment. *Haematologica*
484 2020; **105**: e470.
485 11 de Jong MME, Kellermayer Z, Papazian N, Tahri S, Hofste op Bruinink D, Hoogenboezem
486 R *et al.* The multiple myeloma microenvironment is defined by an inflammatory stromal cell
487 landscape. *Nature Immunology 2021 22:6* 2021; **22**: 769–780.
488 12 de Jong MME, Fokkema C, Papazian N, Czeti Á, Appelman MK, Vermeulen M *et al.* An IL-
489 1β-driven neutrophil–stromal cell axis fosters a BAFF-rich protumor microenvironment in
490 individuals with multiple myeloma. *Nature Immunology 2024* 2024; : 1–14.
491 13 Larrayoz M, Garcia-Barchino MJ, Celay J, Etxebeste A, Jimenez M, Perez C *et al.*
492 Preclinical models for prediction of immunotherapy outcomes and immune evasion
493 mechanisms in genetically heterogeneous multiple myeloma. *Nat Med* 2023; **29**: 632–645.
494 14 Fink EC, McConkey M, Adams DN, Haldar SD, Kennedy JA, Guirguis AA *et al.* Crbn
495 I391V is sufficient to confer in vivo sensitivity to thalidomide and its derivatives in mice.
496 *Blood* 2018; **132**: 1535–1544.
497 15 Ye J, Calvo IA, Cenzano I, Vilas A, Martinez-de-Morentin X, Lasaga M *et al.* Deconvolution
498 of the hematopoietic stem cell microenvironment reveals a high degree of specialization and
499 conservation. *iScience* 2022; **25**: 104225.
500 16 Aibar S, González-Blas CB, Moerman T, Huynh-Thu VA, Imrichova H, Hulselmans G *et al.*
501 SCENIC: Single-cell regulatory network inference and clustering. *Nat Methods* 2017; **14**:
502 1083.

503 17 Sumida TS, Dulberg S, Schupp JC, Lincoln MR, Stillwell HA, Axisa PP *et al.* Type I
504 interferon transcriptional network regulates expression of coinhibitory receptors in human T
505 cells. *Nature Immunology 2022 23:4* 2022; **23**: 632–642.
506 18 Olbromski M, Podhorska-Okołów M, Dzięgiel P. Role of the SOX18 protein in neoplastic
507 processes. *Oncol Lett* 2018; **16**: 1383.
508 19 Yang J, Xu J, Danniel M, Wang X, Wang W, Zeng L *et al.* The interaction between XBP1
509 and eNOS contributes to endothelial cell migration. *Exp Cell Res* 2018; **363**: 262–270.
510 20 Jin Y, Chen K, De Paepe A, Hellqvist E, Krstic AD, Metang L *et al.* Active enhancer and
511 chromatin accessibility landscapes chart the regulatory network of primary multiple
512 myeloma. *Blood* 2018; **131**: 2138–2150.
513 21 Fairfield H, Costa S, Falank C, Farrell M, Murphy CS, D'Amico A *et al.* Multiple Myeloma
514 Cells Alter Adipogenesis, Increase Senescence-Related and Inflammatory Gene Transcript
515 Expression, and Alter Metabolism in Preadipocytes. *Front Oncol* 2021; **10**: 1.
516 22 Fan F, Podar K. The Role of AP-1 Transcription Factors in Plasma Cell Biology and
517 Multiple Myeloma Pathophysiology. *Cancers (Basel)* 2021; **13**.
518 doi:10.3390/CANCERS13102326.
519 23 Chen L, Wang S, Zhou Y, Wu X, Entin I, Epstein J *et al.* Identification of early growth
520 response protein 1 (EGR-1) as a novel target for JUN-induced apoptosis in multiple
521 myeloma. *Blood* 2010; **115**: 61–70.
522 24 Xu G, Liu K, Anderson J, Patrene K, Lentzsch S, Roodman GD *et al.* Expression of XBP1s
523 in bone marrow stromal cells is critical for myeloma cell growth and osteoclast formation.
524 *Blood* 2012; **119**: 4205.
525 25 Huerta-Yepez S, Liu H, Baritaki S, Cebrera-Muñoz MDL, Rivera-Pazos C, Maldonado-
526 Valenzuela A *et al.* Overexpression of Yin Yang 1 in bone marrow-derived human multiple
527 myeloma and its clinical significance. *Int J Oncol* 2014; **45**: 1184–1192.
528 26 Lee M, Cho HJ, Park KS, Jung HY. ELK3 Controls Gastric Cancer Cell Migration and
529 Invasion by Regulating ECM Remodeling-Related Genes. *Int J Mol Sci* 2022; **23**.
530 doi:10.3390/IJMS23073709.
531 27 Dimitrov D, Türei D, Garrido-Rodriguez M, Burmedi PL, Nagai JS, Boys C *et al.*
532 Comparison of methods and resources for cell-cell communication inference from single-cell
533 RNA-Seq data. *Nature Communications 2022 13:1* 2022; **13**: 1–13.
534 28 Benwell CJ, Johnson RT, Taylor JAGE, Price CA, Robinson SD. Endothelial VEGFR
535 Coreceptors Neuropilin-1 and Neuropilin-2 Are Essential for Tumor Angiogenesis. *Cancer*
536 *Research Communications* 2022; **2**: 1626–1640.
537 29 Fan X, Wang Y, Zhang C, Liu L, Yang S, Wang Y *et al.* ADAM9 Expression Is Associate
538 with Glioma Tumor Grade and Histological Type, and Acts as a Prognostic Factor in Lower-
539 Grade Gliomas. *Int J Mol Sci* 2016; **17**. doi:10.3390/IJMS17091276.
540 30 Li YZ, Xie J, Wang RQ, Gao XQ, Liu PJ, Liu J. KLF2 is a clinical diagnostic and treatment
541 biomarker of breast cancer. *Front Cell Dev Biol* 2023; **11**: 1182123.
542 31 Nayak L, Shi H, Atkins GB, Lin Z, Schmaier AH, Jain MK. The thromboprotective effect of
543 bortezomib is dependent on the transcription factor Kruppel-like factor 2 (KLF2). *Blood*
544 2014; **123**: 3828–3831.
545 32 Liu XS, Genet MD, Haines JE, Mehanna EK, Wu S, Chen HIH *et al.* ZBTB7A suppresses
546 melanoma metastasis by transcriptionally repressing MCAM. *Mol Cancer Res* 2015; **13**:
547 1206.
548 33 Xiu L, Zhao Y, Li N, Zeng J, Liu J, Fu Y *et al.* High expression of RARG accelerates
549 ovarian cancer progression by regulating cell proliferation. *Front Oncol* 2022; **12**: 1063031.
550 34 De Stefano V, Larocca A, Carpenedo M, Cavo M, Di Raimondo F, Falanga A *et al.*
551 Thrombosis in multiple myeloma: risk stratification, antithrombotic prophylaxis, and

552 management of acute events. A consensus-based position paper from an ad hoc expert panel.
553 *Haematologica* 2022; **107**: 2536.
554 35 Lu L, Payvandi F, Wu L, Zhang LH, Hariri RJ, Man HW *et al.* The anti-cancer drug
555 lenalidomide inhibits angiogenesis and metastasis via multiple inhibitory effects on
556 endothelial cell function in normoxic and hypoxic conditions. *Microvasc Res* 2009; **77**: 78–
557 86.
558 36 De Luisi A, Ferrucci A, Coluccia AML, Ria R, Moschetta M, De Luca E *et al.* Lenalidomide
559 restrains motility and overangiogenic potential of bone marrow endothelial cells in patients
560 with active multiple myeloma. *Clinical Cancer Research* 2011; **17**: 1935–1946.
561 37 Marine J-C, Jochemsen AG, Lozano G, Levine AJ. MDMX (MDM4), a Promising Target for
562 p53 Reactivation Therapy and Beyond. *Cold Spring Harb Perspect Med* 2016; **6**: a026237.
563 38 Sarıman M, Abacı N, Ekmekçi SS, Çakiris A, Perçin Paçal F, Üstek D *et al.* Investigation of
564 Gene Expressions of Myeloma Cells in the Bone Marrow of Multiple Myeloma Patients by
565 Transcriptome Analysis. *Balkan Med J* 2019; **36**: 23–31.
566 39 Giuliani N, Morandi F, Tagliaferri S, Lazzaretti M, Bonomini S, Crugnola M *et al.* The
567 proteasome inhibitor bortezomib affects osteoblast differentiation in vitro and in vivo in
568 multiple myeloma patients. *Blood* 2007; **110**: 334–338.
569 40 Sekiguchi Y, Ichikawa K, Wakabayashi M, Sugimoto K, Tomita S, Izumi H *et al.* Bone
570 formation following lenalidomide-dexamethasone combination therapy in cases of multiple
571 myeloma refractory to high-dose chemotherapy with bortezomib and autologous peripheral
572 blood stem cell transplantation: report of a case and review of the literature. *Int J Clin Exp*
573 *Pathol* 2015; **8**: 9609.
574 41 Schumacher N, Rose-John S. ADAM17 Activity and IL-6 Trans-Signaling in Inflammation
575 and Cancer. *Cancers (Basel)* 2019; **11**: 1736.
576 42 Abdalla AME, Miao Y, Ming N, Ouyang C. ADAM10 modulates the efficacy of T-cell-
577 mediated therapy in solid tumors. *Immunol Cell Biol* 2024; **102**: 907–923.
578 43 Liu J, Xiao Q, Xiao J, Niu C, Li Y, Zhang X *et al.* Wnt/β-catenin signalling: function,
579 biological mechanisms, and therapeutic opportunities. *Signal Transduction and Targeted*
580 *Therapy 2021 7:1* 2022; **7**: 1–23.
581 44 Simic MK, Mohanty ST, Xiao Y, Cheng TL, Taylor VE, Charlat O *et al.* Multi-Targeting
582 DKK1 and LRP6 Prevents Bone Loss and Improves Fracture Resistance in Multiple
583 Myeloma. *Journal of Bone and Mineral Research* 2023; **38**: 814.
584 45 de Jong MME, Kellermayer Z, Papazian N, Tahri S, op Bruinink DH, Hoogenboezem R *et*
585 *al.* The multiple myeloma microenvironment is defined by an inflammatory stromal cell
586 landscape. *Nat Immunol* 2021; **22**: 769–780.
587 46 Kletukhina S, Neustroeva O, James V, Rizvanov A, Gomzikova M. Role of Mesenchymal
588 Stem Cell-Derived Extracellular Vesicles in Epithelial–Mesenchymal Transition. *Int J Mol*
589 *Sci* 2019; **20**: 4813.
590 47 Cohen YC, Zada M, Wang SY, Bornstein C, David E, Moshe A *et al.* Identification of
591 resistance pathways and therapeutic targets in relapsed multiple myeloma patients through
592 single-cell sequencing. *Nature Medicine 2021 27:3* 2021; **27**: 491–503.
593 48 Ledergor G, Weiner A, Zada M, Wang SY, Cohen YC, Gatt ME *et al.* Single cell dissection
594 of plasma cell heterogeneity in symptomatic and asymptomatic myeloma. *Nature Medicine*
595 *2018 24:12* 2018; **24**: 1867–1876.
596 49 Dutta AK, Alberge JB, Sklavenitis-Pistofidis R, Lightbody ED, Getz G, Ghobrial IM. Single-
597 cell profiling of tumour evolution in multiple myeloma — opportunities for precision
598 medicine. *Nature Reviews Clinical Oncology 2022 19:4* 2022; **19**: 223–236.
599 50 Samur MK, Szalat R, Munshi NC. Single-cell profiling in multiple myeloma: insights,
600 problems, and promises. *Blood* 2023; **142**: 313–324.

51 Tirier SM, Mallm JP, Steiger S, Poos AM, Awwad MHS, Giesen N *et al.* Subclone-specific microenvironmental impact and drug response in refractory multiple myeloma revealed by single-cell transcriptomics. *Nature Communications 2021 12:1* 2021; **12**: 1–16.
52 Sharma NS, Choudhary B. Good Cop, Bad Cop: Profiling the Immune Landscape in Multiple Myeloma. *Biomolecules* 2023; **13**. doi:10.3390/BIOM13111629.
53 John L, Poos AM, Brobeil A, Schinke C, Huhn S, Prokoph N *et al.* Resolving the spatial architecture of myeloma and its microenvironment at the single-cell level. *Nature Communications 2023 14:1* 2023; **14**: 1–17.
54 Pilcher WC, Yao L, Gonzalez-Kozlova E, Pita-Juarez Y, Karagkouni D, Acharya CR *et al.* A single-cell atlas characterizes dysregulation of the bone marrow immune microenvironment associated with outcomes in multiple myeloma. *bioRxiv* 2024; : 2024.05.15.593193.
55 Kellermayer Z, Tahri S, de Jong MME, Papazian N, Fokkema C, Stoetman ECG *et al.* Interferon gamma-mediated prevention of tumor progression in a mouse model of multiple myeloma. *Hemasphere* 2024; **8**. doi:10.1002/HEM3.70047.
56 de Jong MME, Chen L, Raaijmakers MHGP, Cupedo T. Bone marrow inflammation in haematological malignancies. *Nature Reviews Immunology 2024 24:8* 2024; **24**: 543–558.
57 Fotiou D, Katodritou E. From Biology to Clinical Practice: The Bone Marrow Microenvironment in Multiple Myeloma. *Journal of Clinical Medicine 2025, Vol 14, Page 327* 2025; **14**: 327.
58 Pergaris A, Danas E, Goutas D, Sykaras AG, Soranidis A, Theocharis S. The Clinical Impact of the EPH/Ephrin System in Cancer: Unwinding the Thread. *Int J Mol Sci* 2021; **22**. doi:10.3390/IJMS22168412.
59 Chong PSY, Chng WJ, de Mel S. STAT3: A Promising Therapeutic Target in Multiple Myeloma. *Cancers (Basel)* 2019; **11**. doi:10.3390/CANCERS11050731.
60 Ho M, Xiao A, Yi D, Zanwar S, Bianchi G. Treating Multiple Myeloma in the Context of the Bone Marrow Microenvironment. *Current Oncology 2022, Vol 29, Pages 8975-9005* 2022; **29**: 8975–9005.

630 **FIGURE LEGENDS**

631 **Fig. 1. Single-cell transcriptomic profiling of BM murine cells in control, MGUS, and MM.** (A)
632 Experiment overview. Schematic view of experimental workflow for the isolation and scRNA-seq analysis of
633 PC, MSC and EC from control ($YFP_{c\gamma1}$) (pool of 6 mice), MGUS $BI_{c\gamma1}$ (pool of 5 mice), MM $BI_{c\gamma1}$ (pool of 5
634 mice), MGUS $MI_{c\gamma1}$ (pool of 4 mice) and MM $MI_{c\gamma1}$ (pool of 5 mice) murine models. (B) Left panel: UMAP
635 representation of murine BM microenvironment control, MGUS, and MM cells colored by cell clustering after
636 merging samples. Right panels: Original UMAP split into control, MGUS, and MM datasets. (C) Dot plot of
637 canonical markers used to define PC, EC, MSC, erythroblasts, and neutrophils. The dot size reflects the
638 percentage of cells within the cluster expressing each gene, and the color represents the average expression
639 level. (D) UMAP projection showing the distribution of EC from control (n=315 cells), MGUS (n=262 cells),
640 and MM (n=2 060 cells). (E) UMAP visualization of representative canonical markers for EC. (F) UMAP
641 projection showing the distribution of MSC from control (n=132 cells), MGUS (n=143 cells), and MM (n=229
642 cells). (G) UMAP visualization of representative canonical markers for MSC.

643

644 **Fig. 2. Identification of a MM-specific IFN signature in the BME.** (A) UMAP dimension reduction of EC
645 revealing a transcriptionally distinct population in MM. (B) Dot plot visualization of the markers defining EC
646 MM2 cluster. Average gene expression is shown by color intensity, and the percentage of cells expressing
647 each gene is shown by size. (C) Bar charts of enriched GO terms from ORA (adjusted p. value) computed
648 using MM2 cluster markers. The horizontal axis represents the negative of the base 10 logarithm of the adjusted
649 p. value. (D) Heatmap representing z-scaled mean regulon activity score of inferred top specific regulons for
650 each stage. (E) UMAP plot illustrating the distribution of the IFN-related signature in MSC across control,
651 MGUS, and MM. (F) Violin plots showing AUC-score for IFN-related signature within MSC in control,
652 MGUS and MM cells. (G-H) Immunofluorescence (IF) staining of EC (Emcn, red), IFN response genes
653 markers of the MM2 cluster (Gbp2, yellow (G); Isg15, green (H)), and nucleus (DAPI) (blue) in Formalin-
654 Fixed Paraffin-Embedded (FFPE) femurs from Control ($YFP_{c\gamma1}$), MGUS $BI_{c\gamma1}$ and MM $BI_{c\gamma1}$. White arrows
655 point EC $Ecmn^+$ IFN^+ (Gbp2 (G)/Isg15 (H)) in MM $BI_{c\gamma1}$.

656

657 **Fig. 3. A stress pre-vascular state characterizes EC during the MGUS stage.** (A) Heatmap of the DEGs
658 between control, MGUS, and MM cells. Color represents the z-score scaled expression values. (B) Violin plots
659 showing the distribution of expression of genes upregulated in MGUS EC. (C) Volcano plot of the DEGs in
660 MGUS vs. MM EC. The y-axis represents the -log10(p-value), and the x-axis represents the log2(fold change).
661 The dot's color denotes the disease stage for which DEG was detected, with grey dots representing non-
662 significant genes. (D) Significant terms derived from ORA between EC from MGUS and MM. (E) Heatmap
663 representing z-scaled mean regulon activity score of inferred top specific regulons for EC in each stage.
664
665 **Fig. 4. MSC undergo early transcriptional changes during pre-malignant MGUS that persist in**
666 **symptomatic MM.** (A) Heatmap depicting DEGs between MSC in control, MGUS, and MM. Color represents
667 the z-score scaled expression values. (B) Heatmap of significantly downregulated GO terms in MGUS and
668 MM cells compared to control MSC with the associated genes. The green color represents the presence of the
669 gene in each GO term. (C) Volcano plot of the DEGs from the comparison between MSC from control and
670 MGUS. The y-axis represents the -log10(p-value), and the x-axis represents the gene's log2(fold change). The
671 dot's color denotes the disease stage for which DEG was detected, with grey dots representing non-significant
672 genes. (D) Significant terms derived from ORA of MSC from control vs MGUS. (E) Volcano plot of the DEGs
673 in MSC from MGUS vs. MM. (F) Significant terms derived from ORA between MSC from MGUS and MM.
674 (G) Heatmap of mean regulon activity score of significantly enriched regulons in each stage. The color scale
675 represents the z-score of the activity scaled by row.
676
677 **Fig. 5. Altered crosstalk between EC and MSC with malignant PC is potentially associated with**
678 **myeloma development** (A) Heatmap showing the number of predicted cellular interactions between EC, MSC
679 and PC. Block sizes and colors are proportional to the number of ligand-receptor pairs. (B-C) Dot plots of
680 representative ligand-receptor interactions between PC and EC (B) or MSC (C) during disease progression.
681 Dot size and color indicate the interaction's specificity and strength, respectively. (D) Chord diagram showing
682 a shared relevant signaling network between EC, MSC, and malignant PC in the MGUS and MM stages.
683 Colors and width represent signal senders and strength, respectively.
684

685 **Fig. 6. scRNA-seq reveals VRd-induced EC and MSC remodeling in myeloma mice.**

686 (A) Violin plot showing AUC-score for IFN-related signature in EC from Control ($YFP_{c\gamma1}$), MM $BIc_{\gamma1}$ (MM)
687 and MM $BI_{c\gamma1}$-*Crbn*^{I391V} VRd-treated (VRd) mice. (B-C) IF staining of EC (Emcn, red), IFN response genes
688 (Gbp2 (yellow, (B)); Isg15 (green, (C)), and nucleus (DAPI) (blue) in FFPE femurs from MM $BI_{c\gamma1}$ mice (MM)
689 and VRd-treated mice. White arrows point EC Ecmn$^+$ IFN$^+$ (Gbp2 (B)/Isg15 (C)) in MM $BI_{c\gamma1}$. (D) Heatmap
690 showing the expression of stress-related DEGs identified in the comparison between treated and non-treated
691 non-IFN MM EC at different stages of the disease. Color represents the z-score scaled expression values. (E)
692 Significant terms derived from ORA between VRd-treated and untreated non-IFN MM EC. (F) Significant
693 terms derived from ORA of MSC from MM mice before and after VRd treatment. (G) Heatmap projecting the
694 expression of DEGs identified in the comparison between non-treated and treated MSC at different stages of
695 the disease. Color represents the z-score scaled expression values.

696

697 **Fig. 7. Transcriptional dynamics of human MSC during myeloma progression.** (A) Experimental
698 workflow used for the isolation and bulk RNA-seq analysis of human BM MSC. (B) PCA of MSC expression
699 profiles shows clustering by disease stage. The color of the dots represents disease stages. (C) Heatmap
700 showing the expression profiles across samples of DEGs identified in each pairwise comparison along disease
701 progression. (D) GSEA plots for the gene sets 'TNFα signaling via NFκB' (left panel) and 'Interferon gamma
702 response' (right panel) in the comparison between healthy donors (HD)- MSC and MM-MSC. (E) PCA plot
703 showing the MM-IFN signature score in each human sample, previously identified murine BM MM cells. (F-
704 G) IF staining of MSC (CD271, red), IFN response genes (*GBP2*, yellow (F); *ISG15,* green (G)), and nucleus
705 (DAPI) (blue) in archived paraffined human BM biopsies of MM patients with low (MM LOW) and high IFN
706 signal (MM HIGH) in stromal cells (see Supplementary Table 2). White arrows point MSC CD271$^+$ in MM
707 LOW IFN samples, and MSC CD271$^+$ IFN$^+$ (GBP2/ISG15) in MM HIGH IFN samples. (H) Heatmap
708 representing the variation of TF activity score across samples.

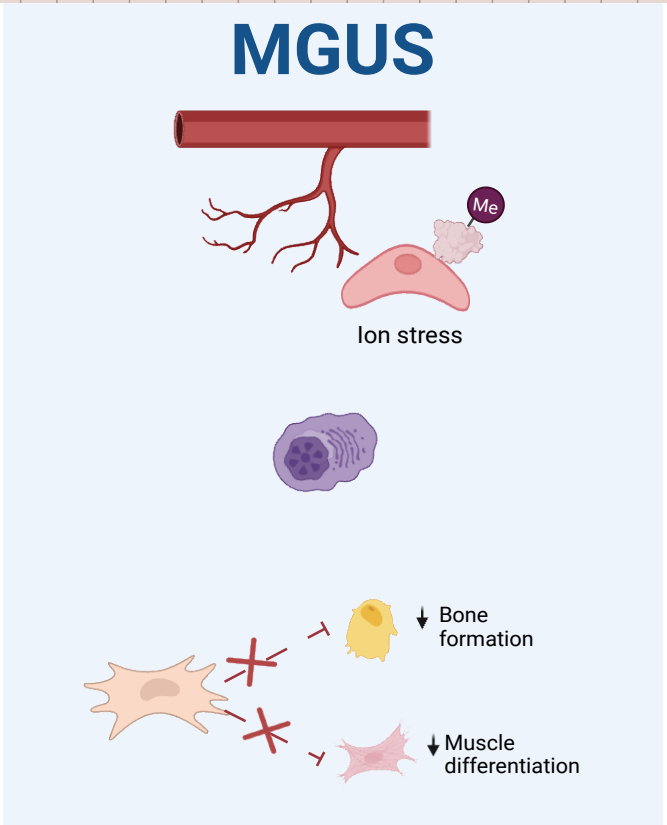
MGUS
Me
Ion stress
Bone formation
Muscle differentiation

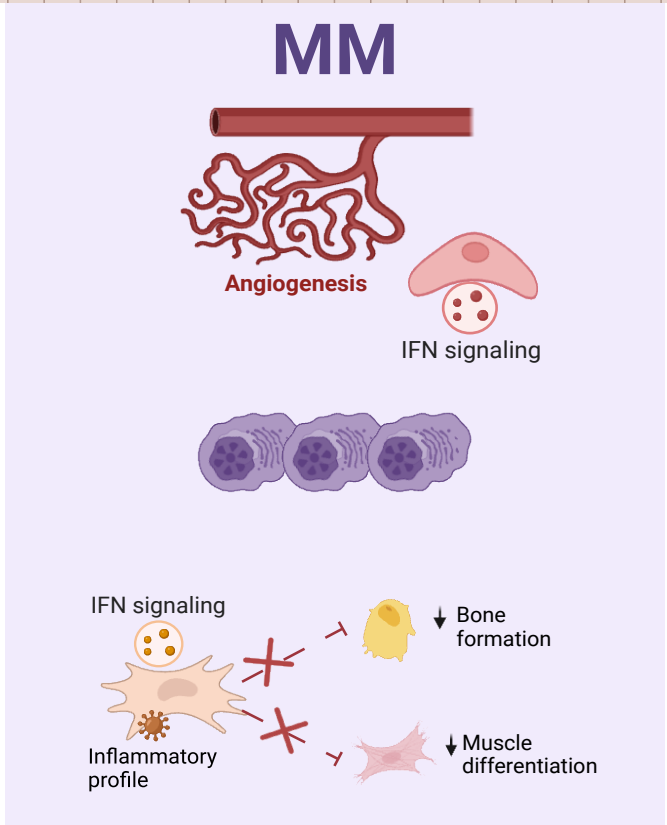
MM
Angiogenesis
IFN signaling
IFN signaling
Bone formation
Inflammatory profile
Muscle differentiation

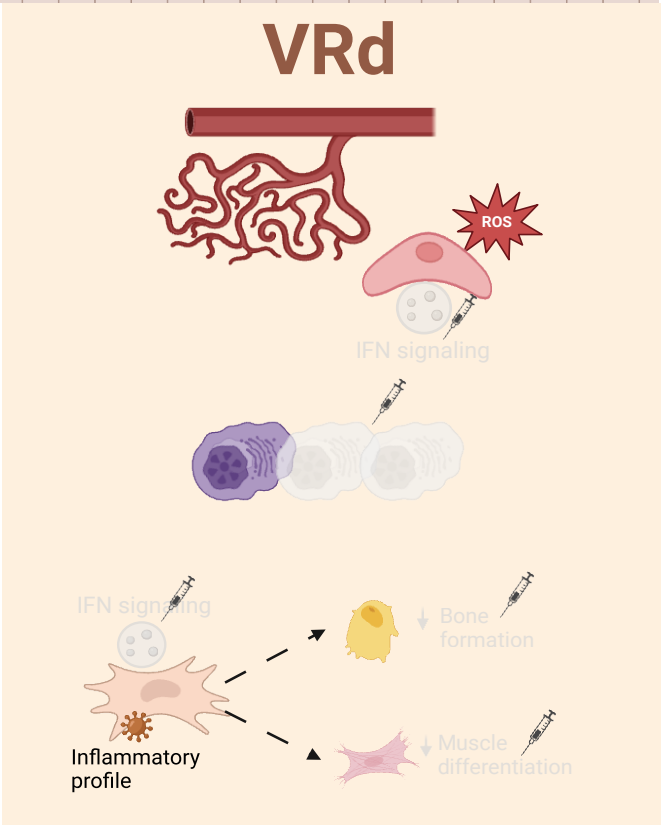
VRd
ROS
IFN signaling
IFN signaling
Bone formation
Inflammatory profile
Muscle differentiation

FIGURE 1

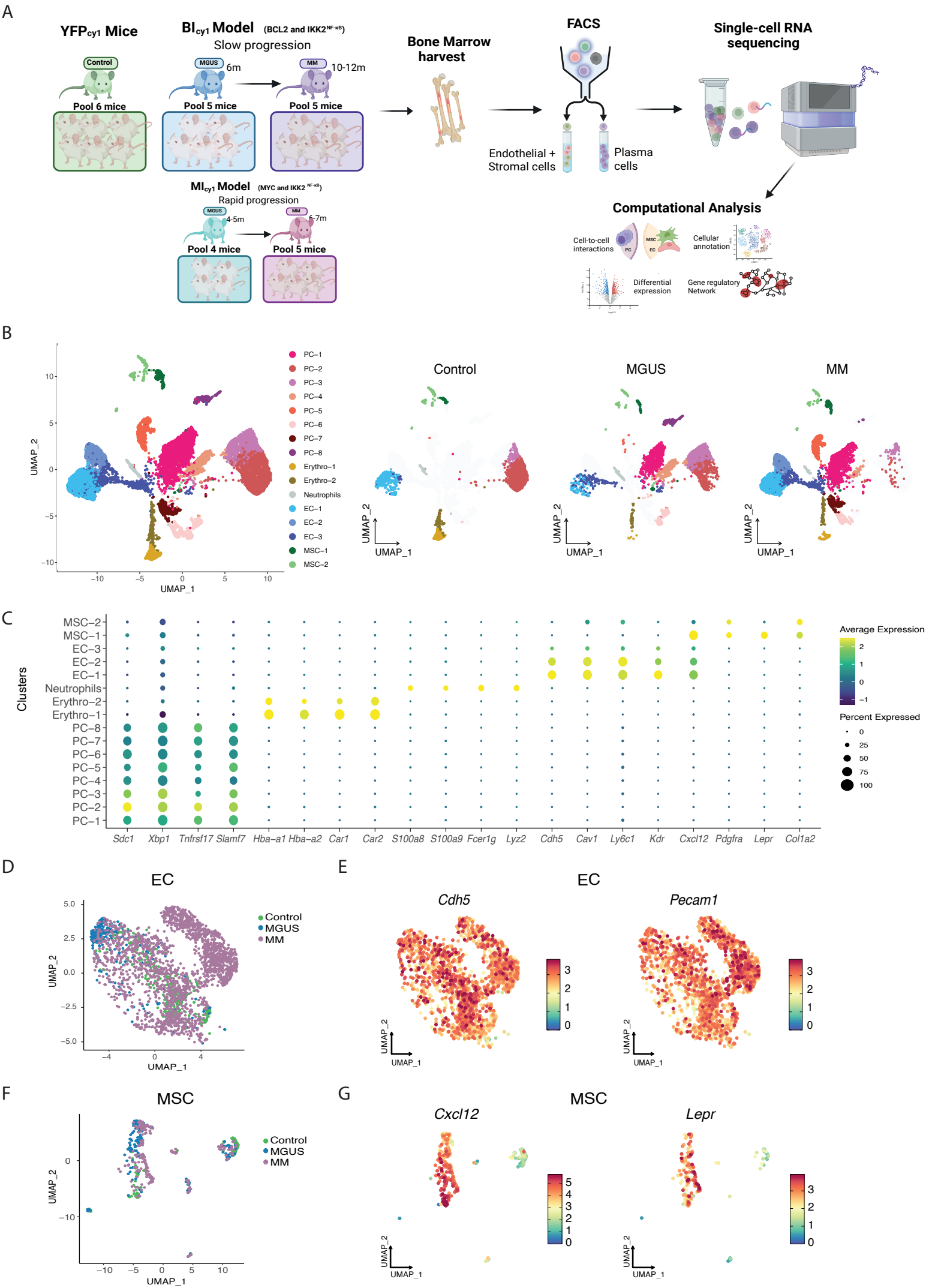
A
YFPcy1 Mice
Control
Pool 6 mice
BIcy1 Model (BCL2 and IKK2NF-κB)
Slow progression
MGUS
6m
MM
10-12m
Pool 5 mice
Pool 5 mice
MIcy1 Model (MYC and IKK2 NF-κB)
Rapid progression
MGUS
4-5m
MM
6-7m
Pool 4 mice
Pool 5 mice
Bone Marrow harvest
FACS
Endothelial + Stromal cells
Plasma cells
Single-cell RNA sequencing
Computational Analysis
Cell-to-cell interactions
Cellular annotation
Differential expression
Gene regulatory Network
B
PC−1
PC−2
PC−3
PC−4
PC−5
PC−6
PC−7
PC−8
Erythro−1
Erythro−2
Neutrophils
EC−1
EC−2
EC−3
MSC−1
MSC−2
UMAP_1
UMAP_2
Control
MGUS
MM
C
Clusters
MSC−2
MSC−1
EC−3
EC−2
EC−1
Neutrophils
Erythro−2
Erythro−1
PC−8
PC−7
PC−6
PC−5
PC−4
PC−3
PC−2
PC−1
Sdc1
Xbp1
Tnfrsf17
Slamf7
Hba−a1
Hba−a2
Car1
Car2
S100a8
S100a9
Fcer1g
Lyz2
Cdh5
Cav1
Ly6c1
Kdr
Cxcl12
Pdgfra
Lepr
Col1a2
Average Expression
Percent Expressed
D
EC
Control
MGUS
MM
UMAP_1
UMAP_2
E
EC
Cdh5
Pecam1
F
MSC
Control
MGUS
MM
G
MSC
Cxcl12
Lepr

FIGURE 2

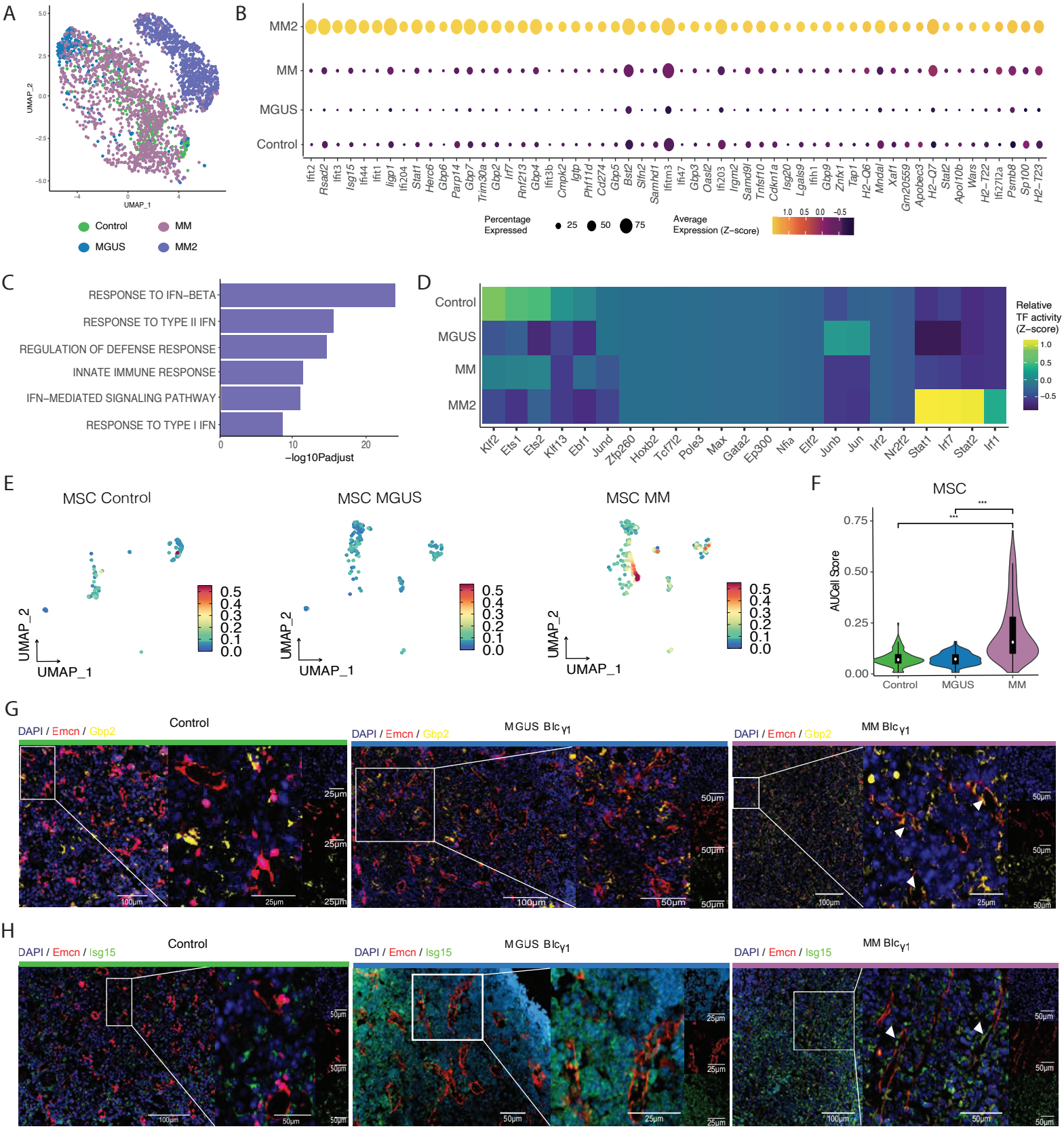
A
UMAP_1
UMAP_2
Control
MM
MGUS
MM2
B
MM2
MM
MGUS
Control
Ifit2 Rsad2 Ifit3 Isg15 Ifi44 Ifit1 Iigp1 Ifi204 Stat1 Herc6 Gbp6 Parp14 Gbp7 Trim30a Gbp2 Irf7 Rnf213 Gbp4 Ifit3b Cmpk2 Igtp Phf11d Cd274 Gbp5 Bst2 Slfn2 Samhd1 Ifitm3 Ifi47 Gbp3 Oasl2 Ifi203 Irgm2 Samd9l Tnfsf10 Cdkn1a Isg20 Lgals9 Ifih1 Gbp9 Znfx1 Tap1 H2-Q6 Mndal Xaf1 Gm20559 Apobec3 H2-Q7 Stat2 Apol10b Wars H2-T22 Ifi27l2a Psmb8 Sp100 H2-T23
Percentage Expressed
25
50
75
Average Expression (Z-score)
1.0 0.5 0.0 −0.5
C
RESPONSE TO IFN-BETA
RESPONSE TO TYPE II IFN
REGULATION OF DEFENSE RESPONSE
INNATE IMMUNE RESPONSE
IFN-MEDIATED SIGNALING PATHWAY
RESPONSE TO TYPE I IFN
0
10
20
−log10Padjust
D
Control
MGUS
MM
MM2
Klf2 Ets1 Ets2 Klf13 Ebf1 Jund Zfp260 Hoxb2 Tcf7l2 Pole3 Max Gata2 Ep300 Nfia Elf2 Junb Jun Irf2 Nr2f2 Stat1 Irf7 Stat2 Irf1
Relative TF activity (Z-score)
1.0
0.5
0.0
−0.5
E
MSC Control
MSC MGUS
MSC MM
UMAP_2
UMAP_1
0.5
0.4
0.3
0.2
0.1
0.0
F
MSC
AUCell Score
0.75
0.50
0.25
0.00
Control
MGUS
MM
G
DAPI / Emcn / Gbp2
Control
MGUS Blc γ1
MM Blc γ1
100µm
25µm
50µm
H
DAPI / Emcn / Isg15
Control
MGUS Blc γ1
MM Blc γ1
100µm
50µm
25µm

FIGURE 3

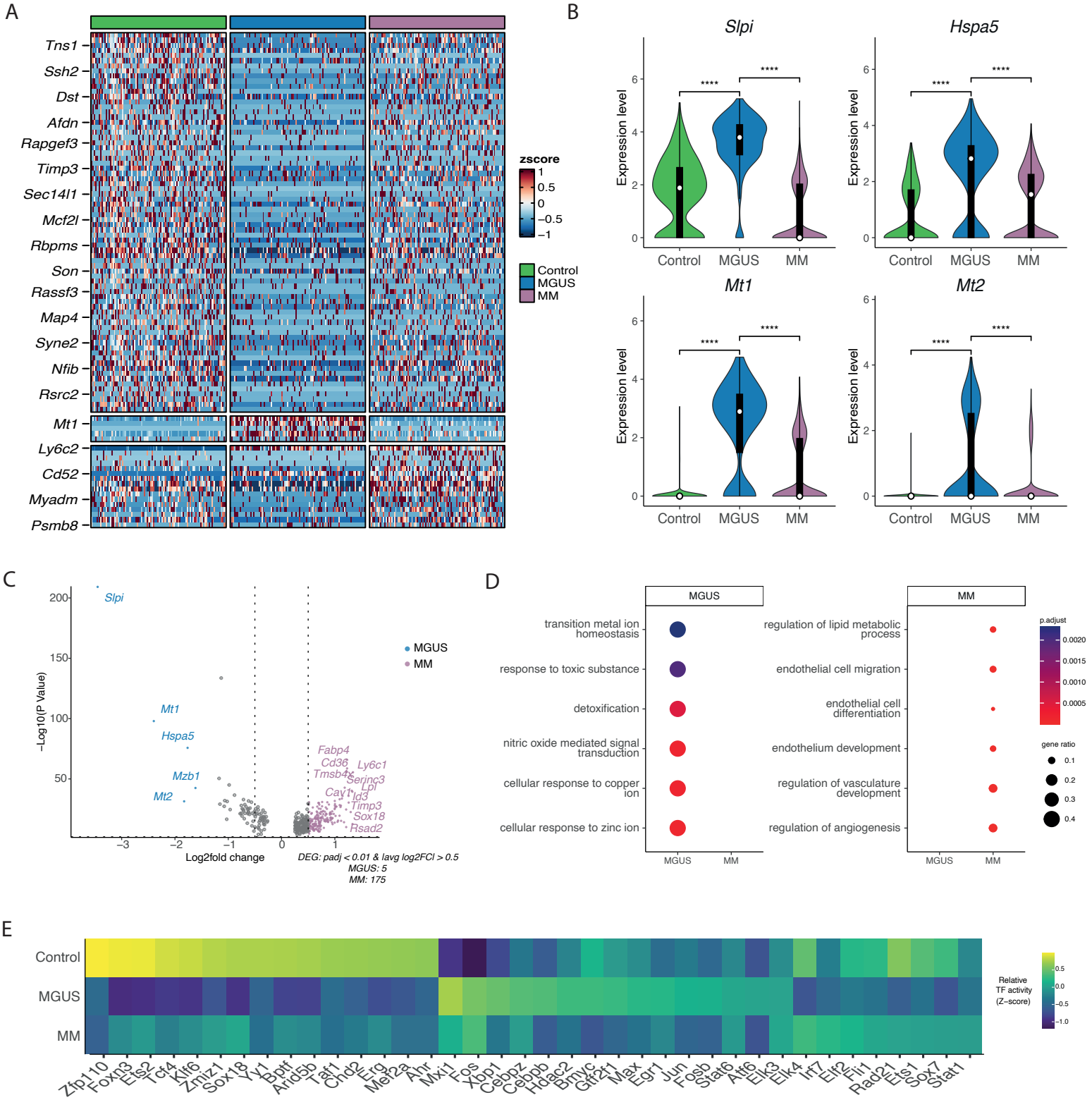
A
Tns1
Ssh2
Dst
Afdn
Rapgef3
Timp3
Sec14l1
Mcf2l
Rbpms
Son
Rassf3
Map4
Syne2
Nfib
Rsrc2
Mt1
Ly6c2
Cd52
Myadm
Psmb8
zscore
1
0.5
0
−0.5
−1
Control
MGUS
MM
B
Slpi
Hspa5
Mt1
Mt2
Expression level
Control
MGUS
MM
****
C
Slpi
Mt1
Hspa5
Mzb1
Mt2
Fabp4
Cd36
Tmsb4x
Ly6c1
Serinc3
Lpl
Cav1
Id3
Timp3
Sox18
Rsad2
MGUS
MM
−Log10(P Value)
Log2fold change
DEG: padj < 0.01 & lavg log2FCl > 0.5
MGUS: 5
MM: 175
D
MGUS
MM
transition metal ion homeostasis
response to toxic substance
detoxification
nitric oxide mediated signal transduction
cellular response to copper ion
cellular response to zinc ion
regulation of lipid metabolic process
endothelial cell migration
endothelial cell differentiation
endothelium development
regulation of vasculature development
regulation of angiogenesis
p.adjust
0.0020
0.0015
0.0010
0.0005
gene ratio
0.1
0.2
0.3
0.4
E
Control
MGUS
MM
Zfp110
Foxn3
Ets2
Tcf4
Klf6
Zmiz1
Sox18
Yy1
Bptf
Arid5b
Taf1
Chd2
Erg
Mef2a
Ahr
Mxi1
Fos
Xbp1
Cebpz
Cebpb
Hdac2
Bmyc
Gtf2f1
Max
Egr1
Jun
Fosb
Stat6
Atf6
Elk3
Elk4
Irf7
Elf2
Fli1
Rad21
Ets1
Sox7
Stat1
Relative TF activity (Z−score)
0.5
0.0
−0.5
−1.0

FIGURE 4

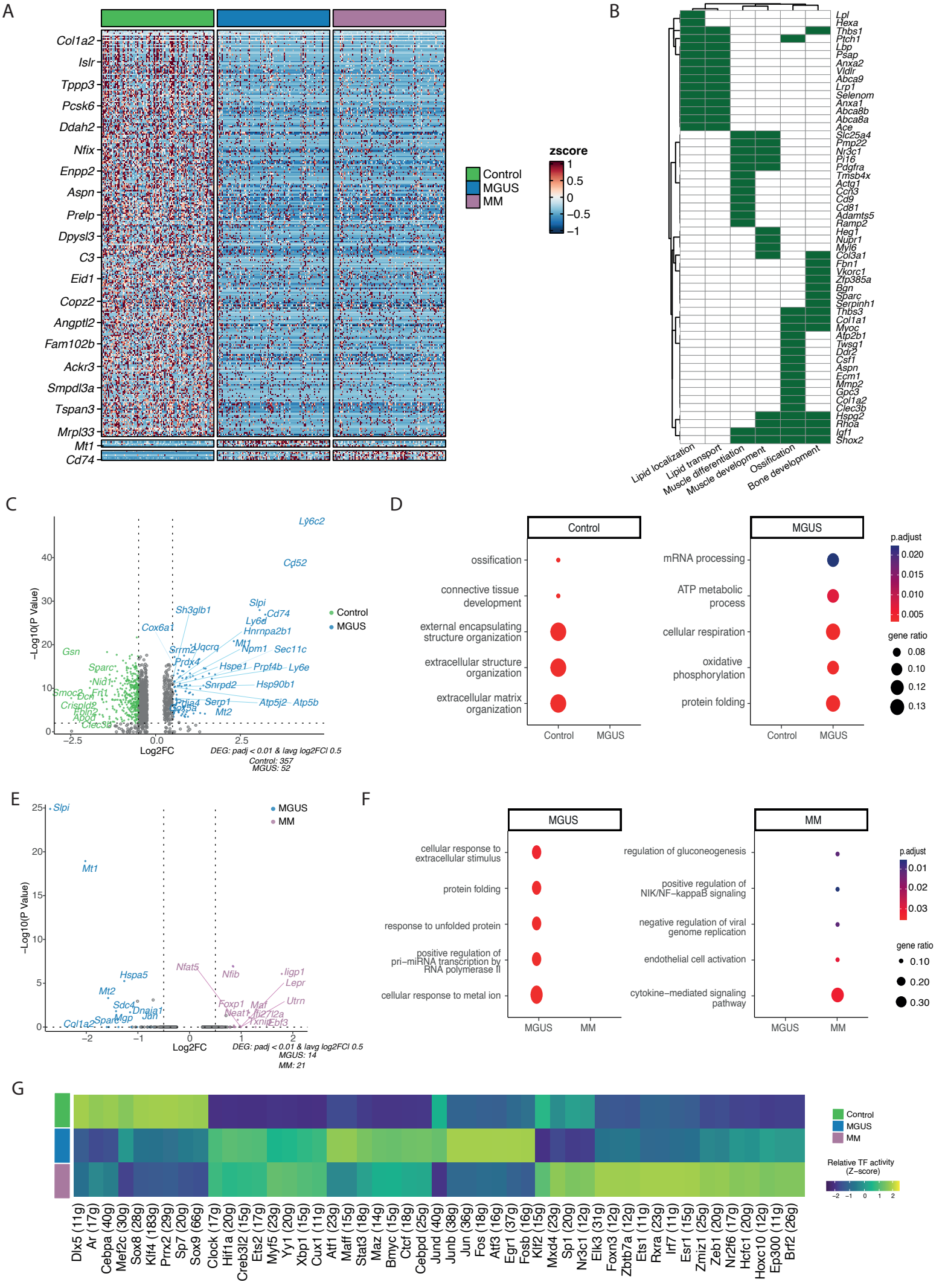
A
Col1a2
Islr
Tppp3
Pcsk6
Ddah2
Nfix
Enpp2
Aspn
Prelp
Dpysl3
C3
Eid1
Copz2
Angptl2
Fam102b
Ackr3
Smpdl3a
Tspan3
Mrpl33
Mt1
Cd74
Control
MGUS
MM
zscore
1
0.5
0
−0.5
−1
B
Lipid localization
Lipid transport
Muscle differentiation
Muscle development
Ossification
Bone development
C
−Log10(P Value)
Log2FC
Control
MGUS
DEG: padj < 0.01 & lavg log2FCl 0.5
Control: 357
MGUS: 52
D
Control
MGUS
ossification
connective tissue development
external encapsulating structure organization
extracellular structure organization
extracellular matrix organization
mRNA processing
ATP metabolic process
cellular respiration
oxidative phosphorylation
protein folding
p.adjust
gene ratio
E
MGUS
MM
−Log10(P Value)
Log2FC
DEG: padj < 0.01 & lavg log2FCl 0.5
MGUS: 14
MM: 21
F
MGUS
MM
cellular response to extracellular stimulus
protein folding
response to unfolded protein
positive regulation of pri−miRNA transcription by RNA polymerase II
cellular response to metal ion
regulation of gluconeogenesis
positive regulation of NIK/NF−kappaB signaling
negative regulation of viral genome replication
endothelial cell activation
cytokine−mediated signaling pathway
p.adjust
gene ratio
G
Control
MGUS
MM
Relative TF activity (Z−score)
Dlx5 (11g)
Ar (17g)
Cebpa (40g)
Mef2c (30g)
Sox8 (28g)
Klf4 (183g)
Prrx2 (29g)
Sp7 (20g)
Sox9 (66g)
Clock (17g)
Hif1a (20g)
Creb3l2 (15g)
Ets2 (17g)
Myf5 (23g)
Yy1 (20g)
Xbp1 (15g)
Cux1 (11g)
Atf1 (23g)
Maff (15g)
Stat3 (18g)
Maz (14g)
Bmyc (15g)
Ctcf (18g)
Cebpd (25g)
Jund (40g)
Junb (38g)
Jun (36g)
Fos (18g)
Atf3 (16g)
Egr1 (37g)
Fosb (16g)
Klf2 (15g)
Mxd4 (23g)
Sp1 (20g)
Nr3c1 (12g)
Elk3 (31g)
Foxn3 (12g)
Zbtb7a (12g)
Ets1 (11g)
Rxra (23g)
Irf7 (11g)
Esr1 (15g)
Zmiz1 (25g)
Zeb1 (20g)
Nr2f6 (17g)
Hcfc1 (20g)
Hoxc10 (12g)
Ep300 (11g)
Brf2 (26g)

FIGURE 5

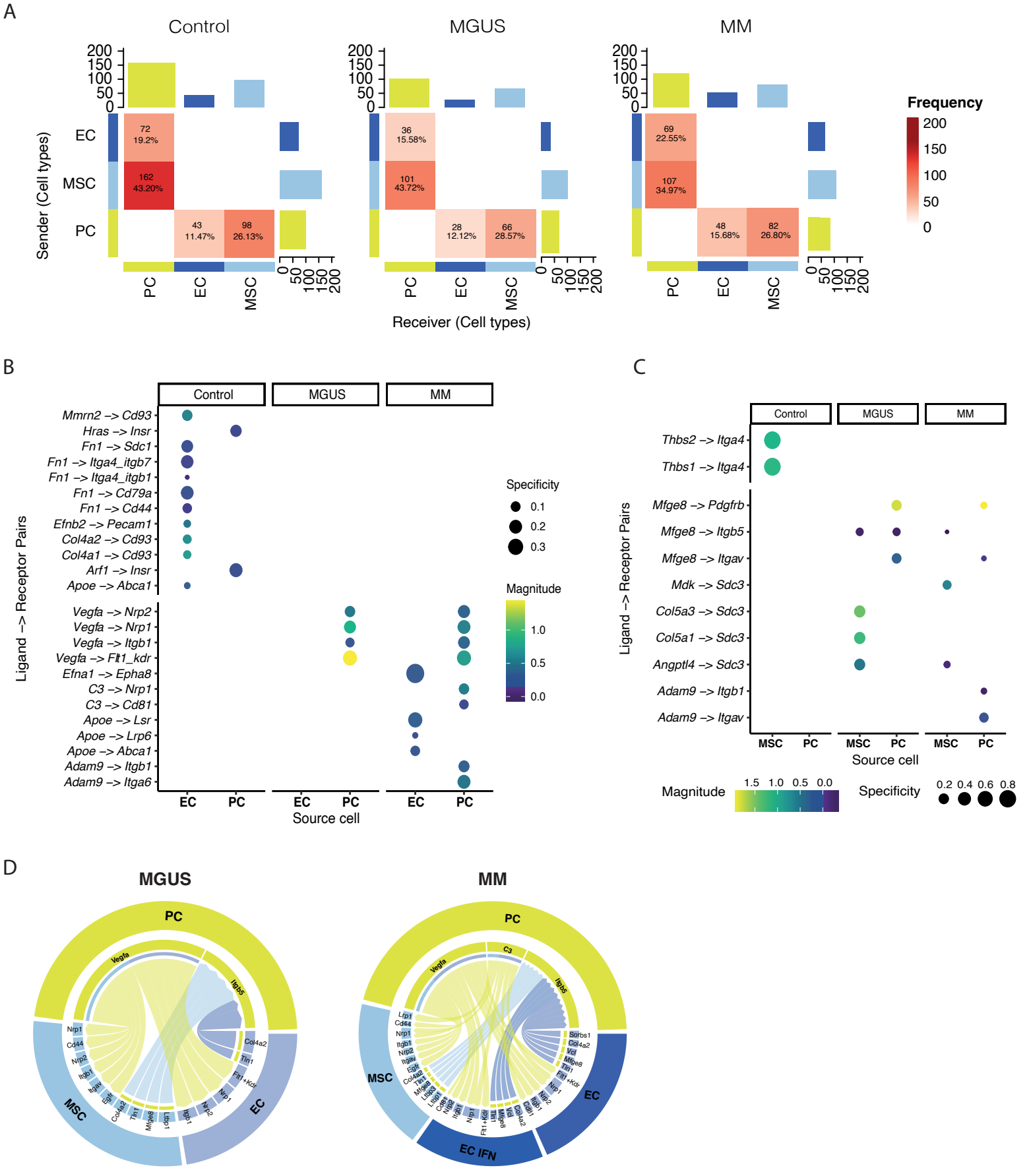
A
Control
MGUS
MM
Sender (Cell types)
EC
MSC
PC
72
19.2%
162
43.20%
43
11.47%
98
26.13%
36
15.58%
101
43.72%
28
12.12%
66
28.57%
69
22.55%
107
34.97%
48
15.68%
82
26.80%
Receiver (Cell types)
Frequency
B
Control
MGUS
MM
Ligand –> Receptor Pairs
Mmrn2 –> Cd93
Hras –> Insr
Fn1 –> Sdc1
Fn1 –> Itga4_itgb7
Fn1 –> Itga4_itgb1
Fn1 –> Cd79a
Fn1 –> Cd44
Efnb2 –> Pecam1
Col4a2 –> Cd93
Col4a1 –> Cd93
Arf1 –> Insr
Apoe –> Abca1
Vegfa –> Nrp2
Vegfa –> Nrp1
Vegfa –> Itgb1
Vegfa –> Flt1_kdr
Efna1 –> Epha8
C3 –> Nrp1
C3 –> Cd81
Apoe –> Lsr
Apoe –> Lrp6
Apoe –> Abca1
Adam9 –> Itgb1
Adam9 –> Itga6
EC
PC
Source cell
Specificity
0.1
0.2
0.3
Magnitude
1.0
0.5
0.0
C
Control
MGUS
MM
Ligand –> Receptor Pairs
Thbs2 –> Itga4
Thbs1 –> Itga4
Mfge8 –> Pdgfrb
Mfge8 –> Itgb5
Mfge8 –> Itgav
Mdk –> Sdc3
Col5a3 –> Sdc3
Col5a1 –> Sdc3
Angptl4 –> Sdc3
Adam9 –> Itgb1
Adam9 –> Itgav
MSC
PC
Source cell
Magnitude
1.5
1.0
0.5
0.0
Specificity
0.2
0.4
0.6
0.8
D
MGUS
MM
PC
MSC
EC
EC IFN
Vegfa
Itgb5
C3
Nrp1
Cd44
Nrp2
Itgb1
Itgav
Egfr
Col4a2
Tln1
Mfge8
Lrp1
Flt1+Kdr
Sorbs1
Vcl

FIGURE 6

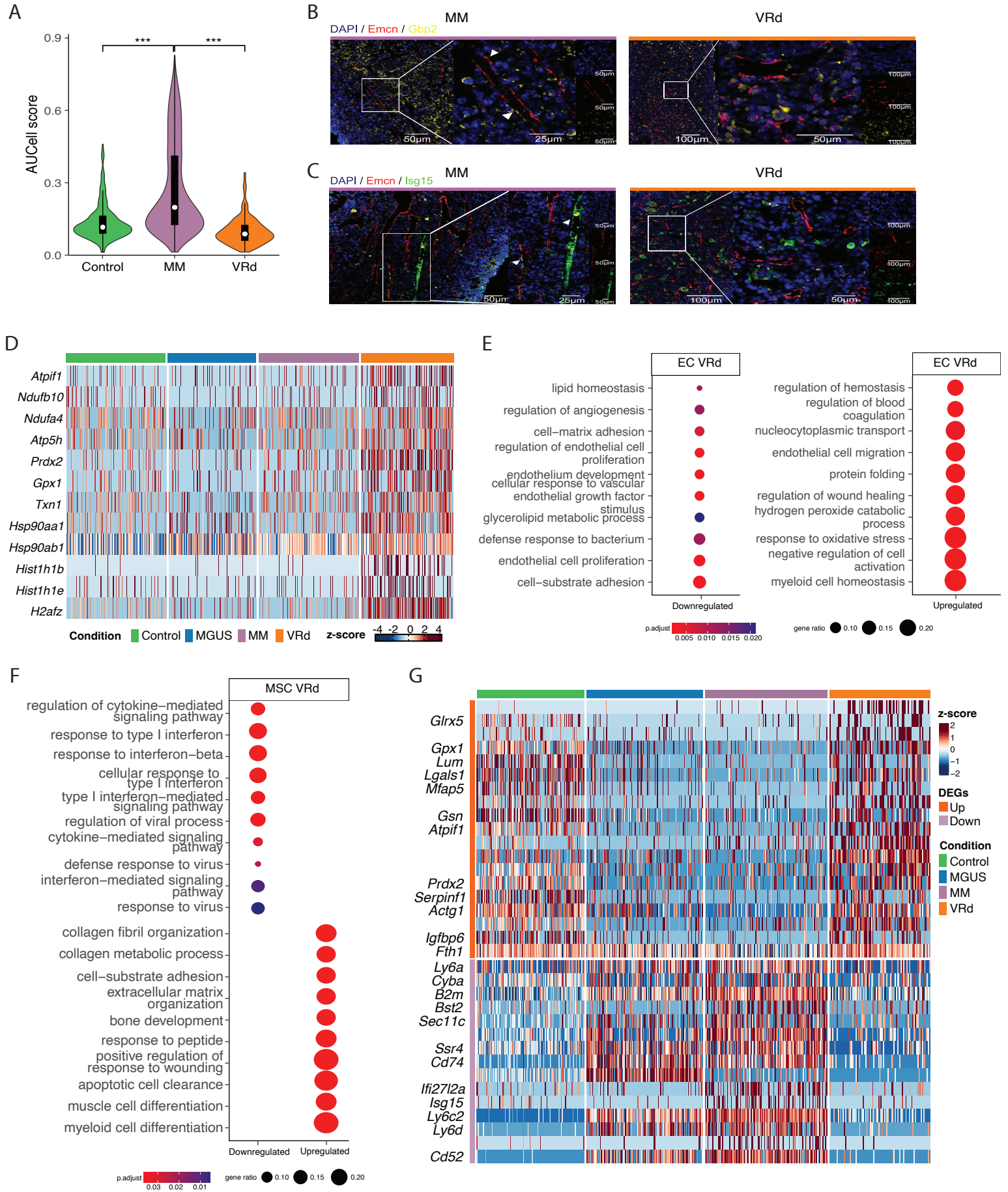
A
AUCell score
0.9
0.6
0.3
0.0
***
***
Control
MM
VRd
B
MM
VRd
DAPI / Emcn / Gbp2
50µm
25µm
100µm
C
MM
VRd
DAPI / Emcn / Isg15
D
Atpif1
Ndufb10
Ndufa4
Atp5h
Prdx2
Gpx1
Txn1
Hsp90aa1
Hsp90ab1
Hist1h1b
Hist1h1e
H2afz
Condition
Control
MGUS
MM
VRd
z-score
-4 -2 0 2 4
E
EC VRd
lipid homeostasis
regulation of angiogenesis
cell–matrix adhesion
regulation of endothelial cell proliferation
endothelium development
cellular response to vascular endothelial growth factor stimulus
glycerolipid metabolic process
defense response to bacterium
endothelial cell proliferation
cell–substrate adhesion
Downregulated
EC VRd
regulation of hemostasis
regulation of blood coagulation
nucleocytoplasmic transport
endothelial cell migration
protein folding
regulation of wound healing
hydrogen peroxide catabolic process
response to oxidative stress
negative regulation of cell activation
myeloid cell homeostasis
Upregulated
p.adjust
0.005 0.010 0.015 0.020
gene ratio
0.10 0.15 0.20
F
MSC VRd
regulation of cytokine–mediated signaling pathway
response to type I interferon
response to interferon–beta
cellular response to type I interferon
type I interferon–mediated signaling pathway
regulation of viral process
cytokine–mediated signaling pathway
defense response to virus
interferon–mediated signaling pathway
response to virus
collagen fibril organization
collagen metabolic process
cell–substrate adhesion
extracellular matrix organization
bone development
response to peptide
positive regulation of response to wounding
apoptotic cell clearance
muscle cell differentiation
myeloid cell differentiation
Downregulated
Upregulated
p.adjust
0.03 0.02 0.01
gene ratio
0.10 0.15 0.20
G
Glrx5
Gpx1
Lum
Lgals1
Mfap5
Gsn
Atpif1
Prdx2
Serpinf1
Actg1
Igfbp6
Fth1
Ly6a
Cyba
B2m
Bst2
Sec11c
Ssr4
Cd74
Ifi27l2a
Isg15
Ly6c2
Ly6d
Cd52
z-score
2
1
0
−1
−2
DEGs
Up
Down
Condition
Control
MGUS
MM
VRd

FIGURE 7

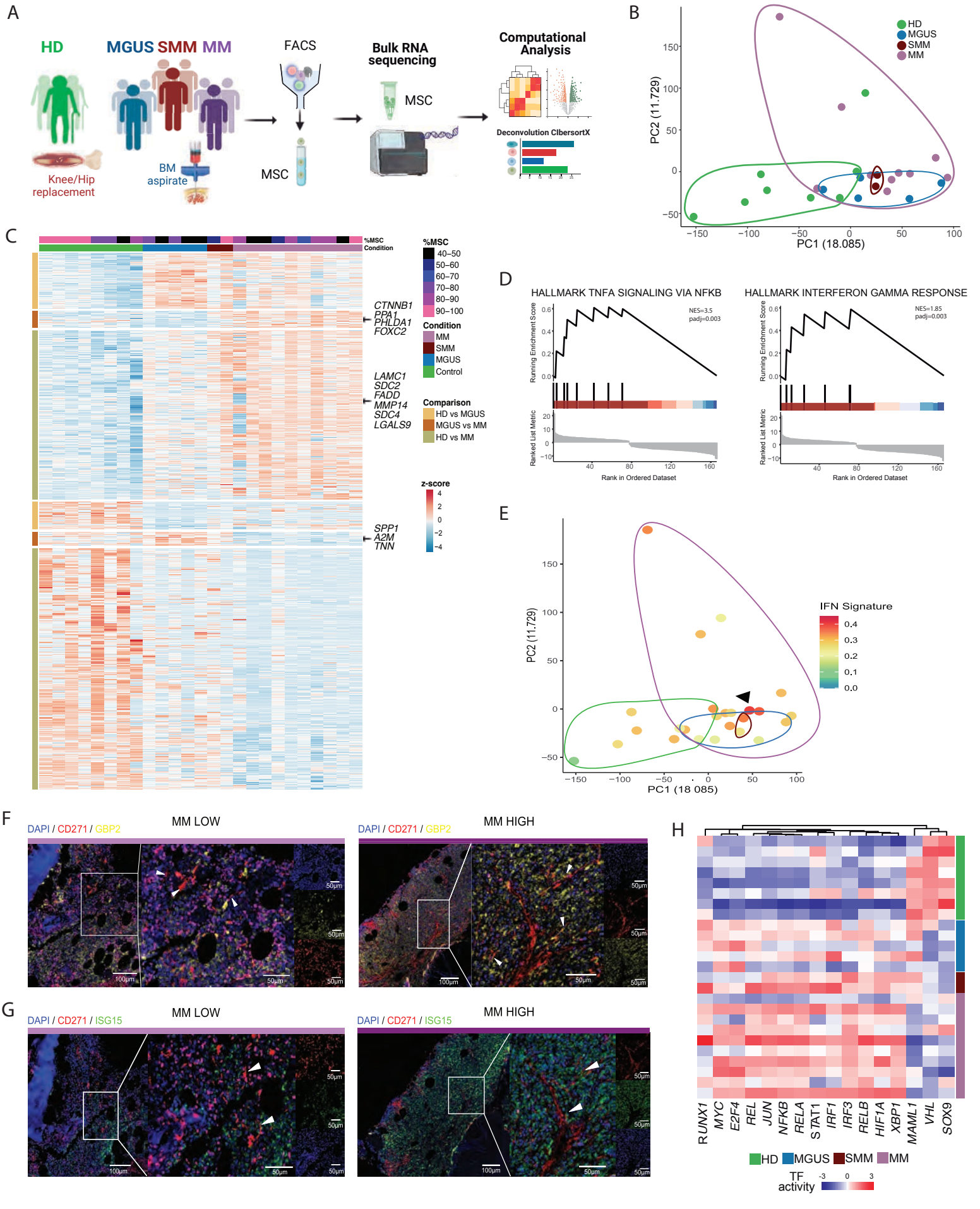
A
HD
MGUS SMM MM
FACS
Bulk RNA sequencing
Computational Analysis
Knee/Hip replacement
BM aspirate
MSC
MSC
Deconvolution CIbersortX
B
HD
MGUS
SMM
MM
PC2 (11.729)
PC1 (18.085)
C
%MSC
Condition
%MSC
40–50
50–60
60–70
70–80
80–90
90–100
Condition
MM
SMM
MGUS
Control
Comparison
HD vs MGUS
MGUS vs MM
HD vs MM
z-score
CTNNB1
PPA1
PHLDA1
FOXC2
LAMC1
SDC2
FADD
MMP14
SDC4
LGALS9
SPP1
A2M
TNN
D
HALLMARK TNFA SIGNALING VIA NFKB
HALLMARK INTERFERON GAMMA RESPONSE
NES=3.5
padj=0.003
NES=1.85
padj=0.003
Running Enrichment Score
Ranked List Metric
Rank in Ordered Dataset
E
IFN Signature
PC2 (11.729)
PC1 (18 085)
F
DAPI / CD271 / GBP2
MM LOW
MM HIGH
G
DAPI / CD271 / ISG15
MM LOW
MM HIGH
H
RUNX1
MYC
E2F4
REL
JUN
NFKB
RELA
STAT1
IRF1
IRF3
RELB
HIF1A
XBP1
MAML1
VHL
SOX9
HD
MGUS
SMM
MM
TF activity